



Chirogenesis and Pfeiffer Effect in Optically Inactive Eu^{III} and Tb^{III} Tris(β -diketonate) Upon Intermolecular Chirality Transfer From Poly- and Monosaccharide Alkyl Esters and α -Pinene: Emerging Circularly Polarized Luminescence (CPL) and Circular Dichroism (CD)

OPEN ACCESS

Edited by:

Keiji Hirose,
Osaka University, Japan

Reviewed by:

Sally Elisabeth Plush,
University of South Australia, Australia
Qionghua Jin,
Capital Normal University, China
Munetaka Iwamura,
University of Toyama, Japan

*Correspondence:

Michiya Fujiki
fujikim@ms.naist.jp;
michiya.fujiki@icloud.com
Abd Jalil Jalilah
jalilahjalil@unimap.edu.my

†ORCID:

Michiya Fujiki
orcid.org/0000-0002-3139-9478
Laibing Wang
orcid.org/0000-0002-3380-7826
Abd Jalil Jalilah
orcid.org/0000-0003-1265-0919

Specialty section:

This article was submitted to
Supramolecular Chemistry,
a section of the journal
Frontiers in Chemistry

Received: 26 April 2020

Accepted: 30 June 2020

Published: 11 August 2020

Citation:

Fujiki M, Wang L, Ogata N,
Asanoma F, Okubo A, Okazaki S,
Kamite H and Jalilah AJ (2020)
Chirogenesis and Pfeiffer Effect in
Optically Inactive Eu^{III} and Tb^{III}
Tris(β -diketonate) Upon Intermolecular
Chirality Transfer From Poly- and
Monosaccharide Alkyl Esters and
 α -Pinene: Emerging Circularly
Polarized Luminescence (CPL) and
Circular Dichroism (CD).
Front. Chem. 8:685.
doi: 10.3389/fchem.2020.00685

Michiya Fujiki^{1*†}, Laibing Wang^{1†}, Nanami Ogata¹, Fumio Asanoma¹, Asuka Okubo¹,
Shun Okazaki¹, Hiroki Kamite¹ and Abd Jalil Jalilah^{1,2,3*†}

¹ Division of Materials Science, Graduate School of Science and Technology, Nara Institute of Science and Technology, Ikoma, Japan, ² School of Materials Engineering, Universiti Malaysia Perlis, Jejawi, Malaysia, ³ Centre of Excellence Frontier Materials Research, Universiti Malaysia Perlis, Kangar, Malaysia

We report emerging circularly polarized luminescence (CPL) at 4*f*-4*f* transitions when lanthanide (Eu^{III} and Tb^{III}) tris(β -diketonate) embedded to cellulose triacetate (**CTA**), cellulose acetate butyrate (**CABu**), *D*-/*L*-glucose pentamethyl esters (**D**-/**L**-**Glu**), and *D*-/*L*-arabinose tetramethyl esters (**D**-/**L**-**Ara**) are in film states. Herein, 6,6,7,7,8,8,8-heptafluoro-2,2-dimethyl-3,5-octanedionate (fod) and 2,2,6,6-tetramethyl-3,5-heptanedione (dpm) were chosen as the β -diketonates. The g_{lum} value of Eu(fod)₃ in **CABu** are +0.0671 at 593 nm (⁵D₀ → ⁷F₁) and -0.0059 at 613 nm (⁵D₀ → ⁷F₂), respectively, while those in **CTA** are +0.0463 and -0.0040 at these transitions, respectively. The g_{lum} value of Tb(fod)₃ in **CABu** are -0.0029 at 490 nm (⁵D₄ → ⁷F₆), +0.0078 at 540 nm (⁵D₄ → ⁷F₅), and -0.0018 at 552 nm (⁵D₄ → ⁷F₅), respectively, while those in **CTA** are -0.0053, +0.0037, and -0.0059 at these transitions, respectively. **D**-/**L**-**Glu** and **D**-/**L**-**Ara** induced weaker g_{lum} values at 4*f*-4*f* transitions of Eu(fod)₃, Tb(fod)₃, and Tb(dpm)₃. For comparison, Tb(dpm)₃ in α -pinene showed clear CPL characteristics, though Eu(dpm)₃ did not. A surplus charge neutralization hypothesis was applied to the origin of attractive intermolecular interactions between the ligands and saccharides. This idea was supported from the concomitant opposite tendency in upfield ¹⁹F-NMR and downfield ¹H-NMR chemical shifts of Eu(fod)₃ and the opposite Mulliken charges between *F*-C bonds (fod) and *H*-C bonds (**CTA** and **D**-/**L**-**Glu**). An analysis of CPL excitation (CPLE) and CPL spectra suggests that (+)- and (-)-sign CPL signals of Eu^{III} and Tb^{III} at different 4*f*-4*f* transitions in the visible region are the same with the (+)- and (-)-sign exhibited by CPLE bands at high energy levels of Eu^{III} and Tb^{III} in the near-UV region.

Keywords: non-covalent interaction, circularly polarized luminescence, circular dichroism, europium, terbium, cellulose, saccharide, terpene

INTRODUCTION

In recent years, controlled chirogenesis led by several scenarios of intermolecular chirality transfer endowed with natural and human-made resources has become the most popular phenomenon allowing for an efficient generation of the desired optically active substances in the realms of organic chemistry (Bosnich, 1967; Hayward and Totty, 1969; Noack, 1969; Soai et al., 2019), supramolecular chemistry (Kobayashi et al., 1993; Huang et al., 1998; Prince et al., 2000; Borovkov et al., 2004; Hembury et al., 2008; Aida et al., 2012; Borovkov, 2014; Liu et al., 2015; Goto et al., 2017), polymer chemistry (Green et al., 1993; Yashima et al., 1995; Nakashima et al., 2001; Kawagoe et al., 2010; Numata and Shinkai, 2011; Lee et al., 2012; Duan et al., 2014; Fujiki, 2014; Wang et al., 2014; Akagi, 2019), and molecular aggregation/colloidal/gel chemistry (Palmans and Meijer, 2007; Isare et al., 2010; George et al., 2011; Mei et al., 2015; Roose et al., 2016; Sang et al., 2019). Particularly, chirogenesis in metal coordination chemistry by the chirality transfer has long been one of the central subjects in inorganic chemistry (Mason and Norman, 1965; Kirschner and Ahmad, 1968; Kirschner and Bakkar, 1982; Mason, 1982; Brittain, 1983, 1989; Riehl and Richardson, 1986; Tsukube and Shinoda, 2002; Di Bari and Salvadori, 2005; Muller, 2009, 2014; Bünzli, 2010; Carr et al., 2012; Tanner, 2013; Miyake, 2014; Kumar et al., 2015; Zinna and Di Bari, 2015; Kono et al., 2016; Longhi et al., 2016; Lunkley et al., 2018; Wong et al., 2019).

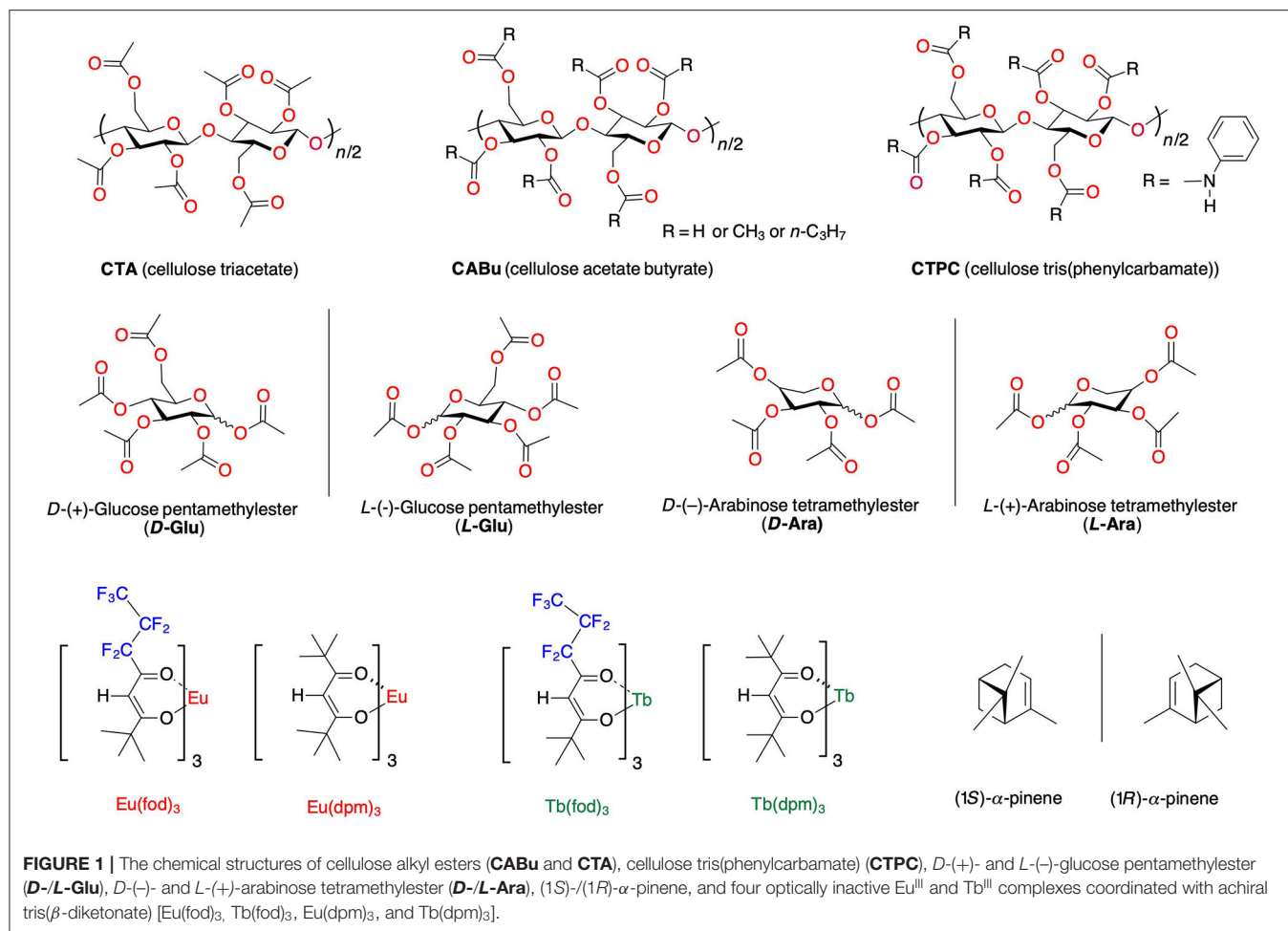
Historically, in 1898, Kipping and Pope investigated the first chirogenesis of *L*-NaClO₃ crystals (*P*₂₁₃ space group) in an enantiomer excess (*ee*) of several % that were preferentially grown in a water solution of *D*-glucose and *D*-mannitol (Kipping and Pope, 1898). In 1919, Perucca found the first chirogenesis of triarylmethane textile dye by observing an anomalous optical rotational dispersion (ORD) in visible region when he dispersed an ORD-silent triarylmethane textile dye in polycrystalline *L*-NaClO₃ (Perucca, 1919; Kahr and Gurney, 2001; Jacoby, 2008; Bing et al., 2010). In the early 1930s, Pfeiffer and Quehl were aware that optical rotation of amino acids increased and/or decreased in the presence of racemic labile metal (Zn²⁺, Cd²⁺, and Ni²⁺) complexes (Pfeiffer and Quehl, 1931, 1932). This anomaly is called as the *Pfeiffer effect* (Mayer and Brasted, 1973; Mason, 1982; Brittain, 1983, 1989; Lunkley et al., 2018).

In 1965, Mason and Norman reported the first circular dichroism (CD) signals at *3d-3d* transitions of Co^{III}(NH₃)₆(ClO₄)₃ in the presence of (+)-diethyl tartrate (Mason and Norman, 1965). In 1977, the first circularly polarized luminescence (CPL) spectra from optically inactive Eu^{III}(fod)₃, Eu^{III}(dpm)₃, Tb^{III}(fod)₃, and other two Eu^{II} complexes dissolved in (*R*)-/(*S*)- α -phenylethylamine are reported by hypothesizing the Pfeiffer effect (fod = 6,6,7,7,8,8,8-heptafluoro-2,2-dimethyl-3,5-octanedionate, dpm: dipivaloylmethane or 2,2,6,6-tetramethyl-3,5-heptanedione) (Brittain and Richardson, 1977a; Brittain, 1980). These pioneering CPL studies further stimulated many researchers to investigate CPL and CD spectroscopic characteristics of optically inactive lanthanide complexes in the presence of amino acids, monosaccharides,

malic acid ascorbic acid, cyclic glycols, DNA, and other chiral chemical influences (Luk and Richardson, 1974; Brittain and Richardson, 1977b; Madaras and Brittain, 1980; Brittain, 1981, 1984; Richardson, 1982; Yan et al., 1982; Huskowska and Riehl, 1995; Muller and Riehl, 2005; Muller, 2009; Iwamura et al., 2012, 2016; Miyake et al., 2014; Wu et al., 2016, 2019; Jalilah et al., 2018; Lunkley et al., 2018; Wu and Bouř, 2018; Taniguchi et al., 2019). An outer-sphere intermolecular interaction between the Δ -/ Λ -mixture lanthanide^{III} (Ln^{III}) complex and the chiral additives is responsible for the equilibrium shift, as detectable by emerging CPL spectra. Richardson et al. evaluated that the barrier heights in Δ - Λ stereomutation between charged M⁺[Eu(dpa)₃]⁻ (M⁺; counter cationic species and dpa; dipicolinate) at the photoexcited state (ES) in achiral solvents are in the range of 12 and 17 kcal mol⁻¹; higher viscosity cosolvents of water-ethylene glycol corresponded to higher barrier heights (Glover-Fischer et al., 1998).

New knowledge and understanding of several weak inter- and intramolecular interactions known as *C-H*/ π , *C-H*/*O-C*, *C-H*/*F-C*, *C-F*/*H-O*, *C-F*/*Si*, and π - π (Nishio et al., 1998; Desiraju and Steiner, 1999; Matsuura et al., 2003; Mele et al., 2003; Tsuzuki et al., 2003; Kim et al., 2004; Mahadevi and Sastry, 2016; Pitts et al., 2017) lead us to hypothesize that multiple point chirality and/or main chain helicity of *non-charged* bioresources impose the capability of non-symmetrical force transfer to *non-charged* achiral or optically inactive chromophores and luminophores. *Non-charged* terpene hydrocarbons, e.g., (*S*)-/(*R*)-limonene, (1*S*)-/(1*R*)- α -pinene, and (1*S*)-/(1*R*)- β -pinene, can efficiently work as chiral liquified scaffolds in the ground state (GS) and the ES of several colloidal π -/ σ -conjugated polymers (Kawagoe et al., 2010; Nakano et al., 2010, 2012; Lee et al., 2012; Fujiki, 2014; Wang et al., 2014), colloidal vinyl polymers bearing azobenzene (Jiang et al., 2015), and *non-charged* Eu(fod)₃ (Figure 1; Jalilah et al., 2018). However, to realize practical photonic applications, solution-processable and/or thermoplastic solid materials are inevitably needed because terpenes are volatile, flammable liquids.

Among solidified chiral bioresources, poly- and monosaccharides are incredible biomaterials that are abundant on earth and have a wide variety of functions (Klemm et al., 2005), e.g., allowing growth and maintenance of homochiral life resulting chiral foods (Coulter, 2016), recognition and sorting of enantiomers (Ikai and Okamoto, 2009), service as a building block of optically active supramolecular complexes (Numata and Shinkai, 2011), and fabrication of liquid crystals, solid films, fibers, sheets, and nano-composites for industrial purposes (Dubois et al., 1998; Henriksson et al., 2007; Wang et al., 2007; Iwatake et al., 2008). More recently, poly- and monosaccharides are excellent chiroptical platforms to generate and boost CD/CPL/circularly polarized reflection bands because of their helicoidal and cholesteric higher-order structures (Wilts et al., 2017; De La Cruz et al., 2018; Yu et al., 2018, 2019; Zheng et al., 2018). We have proved that three cellulose derivatives (cellulose triacetate (CTA), cellulose acetate butyrate (CABu), and cellulose tris(phenyl carbamate) (CTPC) in Figure 1 possess



an efficient ambidextrous scaffolding capability toward CD-inactive oligo- and polyfluorenes, leading to the corresponding (+)- or (-)-sign CPL-active/CD-active species as the solid film states (Guo et al., 2017, 2018).

These results encourage us to propose that **CTA**, **CABu**, *D*-/*L*-glucose permethyl esters (**D-Glu/L-Glu**), and *D*-/*L*-arabinose permethyl esters (**D-Ara/L-Ara**) should work as chirality transferring solid platforms, enabling several optically inactive and/or racemic Eu^{III} and Tb^{III} complexes to the corresponding CPL-active/CD-active, non-racemic species (Figure 1). For comparison, we tested the chirality transfer capability of (1*S*)/(1*R*)-α-pinene as chiral liquid molecules to Eu(dpm)₃ and Tb(dpm)₃.

Herein, we showcase that Eu(fod)₃, Tb(fod)₃, and Tb(dpm)₃, except Eu(dpm)₃ commonly exhibited CPL signals at 4*f*-4*f* transitions and CD bands due to *n*-π*/π-π* transitions of the ligands when **CABu**, **CTA**, **D-Glu/L-Glu**, and **D-Ara/L-Ara** were employed as embedding films. In α-pinene, although Tb(dpm)₃ showed clear CPL characteristics, Eu(dpm)₃ did not. Unresolved inherent nature between Eu^{III} and Tb^{III} causes considerable differences of CPL characteristics as well as emission wavelengths at 4*f*-4*f* transitions. Although the current *g*_{lum} values of our

CPL-active lanthanide complex in the films are not very outstanding, the hypothesis of these non-covalent weak chiral intermolecular interactions in the ES and GS led us to freely design solution processible CPL- and/or CD-functioned composite films made of several optically inactive lanthanide complexes coordinated with achiral organic ligands upon chirality/helicity transfer of inexpensive soluble polysaccharide, oligosaccharide, and monosaccharide derivatives as the solidified chiral bioresources, in addition to a conventional multi-step synthesis of optically active lanthanide complexes coordinated with chiral ligands designed strategically.

EXPERIMENTAL

Materials

CTA and CABu

CTA (Wako Pure Chemicals, Osaka, Japan) and **CABu** (Sigma-Aldrich Japan, Tokyo, Japan) were used without further purification (Figures S1, S2, SM). Chloroform, tetrahydrofuran (THF), methanol (MeOH), and other solvents (Dojindo, Kumamoto, Japan) were used as received. CDCl₃ and hexafluorobenzene (C₆F₆) were purchased from Stable Isotope

Lab (SIL) (Japanese vendor, Wako Pure Chemicals) and Wako Pure Chemicals, respectively. (1S)- and (1R)- α -Pinene (Tokyo Chemical Industry (TCI), Tokyo, Japan) were purified by distillation in a reduced pressure.

Monosaccharide Permethylesters

L-(-)-Glu. To a mixture of L-(-)-glucose (0.5 g) and stoichiometric acetic anhydride (4 mL), freshly dried Cu(OTf)₂ (0.03 mol % of L-(-)-glucose) at 0°C was added under nitrogen [Scheme S1 in Supplementary Materials (SM)]. The mixture was stirred for 1 h in an ice bath and then stirred at room temperature for 12 h. Methanol (5 mL) was slowly added to quench the acylation reaction, and the mixture was stirred for another 0.5 h, followed by evaporation under reduced pressure. Chloroform (25 mL) was added to dissolve the residue, and the mixture was consecutively washed twice with saturated NaHCO₃ brine and water, respectively. The organic layer was dried over anhydrous Na₂SO₄, and the mixture was filtered. The filtrate was concentrated in a vacuum and purified by silica gel column chromatography, and eluted with petroleum ether/ethyl acetate (v/v, 50/1) to yield a white powder (yield: 0.42 g, 70%; Analysis: calculated (%) for C₁₆H₂₂O₁₁: C, 49.23; H, 5.68; found (%): C, 49.53; H, 5.43. ¹H-NMR (in CDCl₃), FT-IR (onto CaF₂) and ESI (positive mode)-MS spectra of L-Glu and D-Glu are shown in Figure S3, SM and Figure S4, SM, respectively. Elemental analysis of L-Glu and D-Glu are given in Figure S5, SM.

D-(+)-Glu. Donated from Prof. Wei Zhang (Soochow University, China) prepared by a similar method. ¹H-NMR, FT-IR, and ESI (positive mode) MS spectra are displayed in Figure S4, SM. Solid-state ¹³C-NMR and ¹H-NMR in CDCl₃ solution are shown in Figures 5, 8A, respectively. Analysis: Calcd (%) for C₁₆H₂₂O₁₁: C, 49.23; H, 5.68; Found (%): C, 49.51; H, 5.40.

D-Ara and L-Ara. D-(-)-Arabinose tetramethyl ester and L-(+)-arabinose tetramethyl ester were synthesized utilizing the same procedure as described for the synthesis of L-Glu. A viscous liquid was obtained as D-Ara. Yield: 2.4 g, 32%. Analysis for D-Ara: Calcd (%) for C₁₃H₁₈O₉: C, 49.06; H, 5.70, Found (%): C, 48.97; H, 5.56. L-Ara. Yield (2.4 g, 32%). Analysis: Calcd (%) for C₁₃H₁₈O₉: C, 49.06; H, 5.70, Found (%): C, 49.01; H, 5.60. ¹H-NMR, FT-IR, and ESI-MS (positive mode) spectra of D-Ara and L-Ara are shown in Figures S6, S7, SM, respectively. The results of the elemental analysis of L-Ara and D-Ara are shown in Figure S8, SM.

Tb(fod)₃

The starting material, 0.19 g (0.74 mmol) of TbCl₃ (99% purity, Sigma-Aldrich, now Merck) was dissolved in the minimum amount of methanol (3.0 mL), and 1,1,1,2,2,3,3-heptafluoro-7,7-dimethyl-4,6-octanedione (Hfod, 0.636 g (2.15 mmol, 0.5 mL), TCI) was adjusted to pH 5–6 by adding the required amount of aqueous NaOH solution. The above two solutions were mixed by vigorous stirring with a magnetic stir bar for 10 min, followed by addition of 200 mL distilled water dropwise into the solution. A pale-yellow Tb(fod)₃ was precipitated under vigorous stirring with a magnetic bar for 12 h. The crude product adhered to the bottom of the reaction vessel was purified by a short-column

silica gel chromatography (Wakogel C-200, Chart S1 in SI) as shown below, with chloroform as an eluent to yield a pale yellow oil, followed by drying in a vacuum oven 90°C to obtain a white solid. Yield, 200 mg (40%). The purification of Tb(fod)₃ using a 5 mL pipette tip made of polypropylene, as a short-column apparatus, is illustrated below. Analysis: Calcd (%) for C₃₀H₃₀F₂₁O₆Tb: C, 34.50; H, 2.90. Found (%): C, 34.58; H, 2.80. The elemental analysis suggested that Tb(fod)₃ has no water adducts.

Before we utilized the purification method (see Chart S1, SM) for Tb(fod)₃, we were aware of some impurity peaks approximately 450 nm in the PL spectrum of Tb(fod)₃. After the purification by silica gel column chromatography and elution with chloroform, we obtained a pure Tb(fod)₃ (based on the expected fluorescent emission spectrum). ¹H-NMR (CDCl₃), ¹⁹F-NMR (CDCl₃), FT-IR (CaF₂), and ESI-MS (positive mode) spectra and elemental analysis of Tb(fod)₃ are shown in Figure S9, SM.

Other Lanthanide Complexes

Eu(fod)₃, Eu(dpm)₃, and Tb(dpm)₃ were purchased from Sigma-Aldrich-Merck, TCI, and Sigma-Aldrich-Merck, respectively, and were used as received. ¹H-NMR (CDCl₃) and FT-IR spectra of Eu(fod)₃ are shown in Figure S10, SM. ¹H-NMR and FT-IR spectra of Eu(dpm)₃ are shown in Figure S11, SM. ¹H- and ¹⁹F-NMR (CDCl₃) and FT-IR (CaF₂) spectra of Tb(dpm)₃ are shown in Figure S12, SM.

Instrumentation

The UV-vis and CD spectra of the solutions were measured with a JASCO J-820 spectropolarimeter (Hachioji-Tokyo, Japan) equipped with Peltier-controlled housing units. Synthetic quartz (SQ) cuvette with a 10-mm path length (scanning rate: 100 nm min⁻¹; bandwidth: 1.0 nm; response time: 1.0 s; 0.5-nm interval sampling; single accumulation) at 25°C were used. To avoid second- and third-order stray light due to diffraction grating, CPL and PL spectra were recorded on a JASCO CPL-200, that was designed as a prism-based spectrofluoropolarimeter with a forward scattering of 0° angle equipped with focusing and collecting lenses, and a manually movable film holder onto an optical rail enables to adjust the best focal point to maximize CPL/PL signal amplitudes. Measurement conditions were bandwidths of 10 nm for excitation and emission, a scanning rate of 100 nm min⁻¹, and a data sampling of 0.5 nm interval. IR spectra were measured on CaF₂ plate using a Horiba FT-730 Fourier-transform (FT) infrared (IR) spectrometer (Horiba, Kyoto, Japan) over a wavenumber range between 800 and 4,000 cm⁻¹ with a resolution of 2 cm⁻¹ and a scanning speed of 5 mm s⁻¹ for 128 scans and a Perkin-Elmer Spectrum One/100 FT-IR spectrometer (Winter Street Waltham, MA 02451, USA) over a wavenumber range between 900 and 4,000 cm⁻¹ with a resolution of 4 cm⁻¹ for 64 scans. Electrospray ionization mass spectrometry (ESI-MS) was conducted with a JEOL (Akishima, Tokyo, Japan) AccuTOF JMS-T100 LC mass spectrometer (accelerating voltage,

10 kV). Electron ionization mass spectrometry with high-resolution (HR-EI-MS) mode was recorded with a JEOL JMS-700 double-focusing mass spectrometer (accelerating voltage, 10 kV). The ionic species were often attached with Na^+ ion. The hybridized polymers were characterized by a JEOL JNM-ECX400 cross-polarization (CP) magic-angle-spinning (MAS) solid-state (ss)- $^{13}\text{C}\{\text{H}\}$ -FT-NMR spectrometer (resonance frequency 100.5 MHz, contact time 2.0 ms, 550 scans, relaxation delay 5.0 s, spinning 8.0 kHz, repetition time 5.05 s). Elemental analysis was performed on a Perkin-Elmer 2400II CHNS/O. The solution ^1H - and ^{19}F -FT-NMR spectra were recorded on the JEOL ECP-400 spectrometer. The resonance frequencies of ^{19}F - and ^1H -NMR are 376 MHz and 400 MHz, respectively. Representative measurement conditions for ^{19}F -NMR spectra had an acquisition time of 0.432 sec, 64 acquisitions, a relaxation delay of 4.0 sec, at a temperature of $\sim 20^\circ\text{C}$, a pulse angle of 45° and a pulse width of 7.0 sec were used. Raw NMR data were processed and analyzed by JEOL Delta (Ver. 5) software. Hexafluorobenzene (HFB, -163.0 ppm) and tetramethylsilane (Me_4Si , 0.0 ppm) were used as internal standards for the ^{19}F - and ^1H -NMR measurements, respectively. Photodynamic decay of six solid films ($\text{Eu}(\text{fod})_3$ with **CTA** and **CABu** (detected at 610–620 nm), $\text{Eu}(\text{dpm})_3$ with **CTA** and **CABu** (detected at 610–620 nm), and $\text{Tb}(\text{dpm})_3$ with **CTA** and **CABu** (detected at 542–551 nm) excited by an N_2 laser (Usho KEC-160; wavelength 337.1 nm; pulse width 600 ps; 10 Hz) were measured with the help of streak camera (Hamamatsu, picosecond fluorescence measurement system C4780 with Grating 150 lines per mm and slit width 100 μm). The 337.1 nm of N_2 laser source was used to excite shoulder UV/CD signals of the lanthanide complexes. Photodynamic measurements of other Eu^{III} and Tb^{III} complexes in the *D*-/*L*-**Glu** and *D*-/*L*-**Ara** films excited at 337.1 nm were not successful. For simplicity, the emission lifetime was evaluated by single exponential decay analysis. Quantum yields of the Eu^{III} and Tb^{III} complexes in the solid films were not obtained due to lack of an integrating sphere. The all processed data saved as raw text data were re-organized by KaleidaGraph ver. 4.53 (Synergy software, Reading, PA 19606, USA).

Preparation of the Hybridized Films

In fabricating the hybridized film, 10 mg of lanthanide complexes and 20 mg of saccharide derivatives (**Glu** and **Ara**) or cellulose derivatives (**CABu** and **CTA**) were completely dissolved in 1.0 mL of the desired solvent (chloroform or tetrahydrofuran (THF)) at ambient temperature. The hybridized film was deposited onto a polished circular quartz plate or borosilicate glass (Tempax Float[®], Schott AG, Germany) (25 mm in diameter and 1 mm in thickness) by spin coating using a spin coater (MIKASA, MS-B100, Tokyo, Japan), then, 800 μL of the solution was placed onto the center of the plate and spun at 1,500 rpm for 60 s. The films on the glass were attached on both sides (front and back surfaces) to ensure an *optically symmetrical geometry* with air-sample-(quartz or borosilicate substrate)-sample-air contact by spin coating chloroform or THF solutions that consist of saccharides (chiral host) and lanthanide complex (achiral guest) (Guo et al., 2017, 2018; Yamada et al., 2018). Although the

film thicknesses of both sides were not determined, we assumed to be on the order of several μm for each. The hybridized double-side coating films were scattering-free and transparent by the naked eye. To measure CPL/PL/CPL/PLE/CD/UV-visible spectra, the optical density of the double-side coating specimen was controlled to 0.3–1.0 in the range of 280 and 330 nm. CD, CPL, and CPLE spectra of the hybridized films were measured at ambient temperature (24 – 26°C). The double-sided coating in the symmetrical optical geometry avoids chiroptical inversion artifacts that could be originated from linear dichroism induced by mechanical stress on anisotropic specimens due to spin coating. Based on our experience, single-side coating in the dissymmetrical optical geometry can often cause artifact inversion in signs of CPL and CD signals. In the case of single-side coating, the probability of the chiroptical sign inversion was approximately 2–3 out of 10, while double-side coating prevented the artifact origin sign inversion.

RESULTS AND DISCUSSION

The chirogenesis characteristics of oligo-/polyfluorenes originate from rotatable C–C bonds between fluorene rings and from C–O/C–C bonds of the cellulose derivatives (**Figure 1**) (Guo et al., 2017, 2018; Yamada et al., 2018) in the GS and ES because rotational barrier heights of the single bonds are as small as 1.5–2.5 kcal mol⁻¹. Eu^{III} and Tb^{III} complexes with three fod ligands should coexist as racemic mixtures of *D*-/*L*-species of C_3 -symmetrical facial (*fac*)- and C_1 -meridional (*mer*) motifs (Brittain and Richardson, 1977a; Jalilah et al., 2018), while even Eu^{III} and Tb^{III} with three dpm should coexist as a racemic mixture of *D*-/*L*-species of D_3 -geometry. Although barrier heights of *D*-*L* stereomutation and/or *fac*-*mer* isomerisms are considerably high on the order of 10–20 kcal mol⁻¹ (Glover-Fischer et al., 1998; Carr et al., 2012; Miyake, 2014), multiple intermolecular *C*-*H*/*O*-*C*, *C*-*H*/ π , and *C*-*H*/*F*-*C* interactions (Murray-Rust et al., 1983; Nishio et al., 1998; Desiraju and Steiner, 1999; Tsuzuki et al., 2003; Yuasa et al., 2011; Koiso et al., 2017; Jalilah et al., 2018) should overcome the barriers when solidified matrices are employed. Note that solidified matrices are regarded as solid-like solvents with a very high viscosity. In this work, we applied a double-side, spin-coating technique (Guo et al., 2017, 2018) to fabricate CPL-/CD-functioned films deposited onto fused quartz and/or borosilicate glass to obtain artifact-free CPL/photoluminescence (PL), CPL/PL excitation (PLE), and CD/UV-visible spectra. CPL and CPL spectral characterizations of Eu^{III} and Tb^{III} at 4*f*-4*f* transitions were assigned based on the literature (Fulgêncio et al., 2012; Tanner, 2013; Binnemans, 2015; de Queiroz et al., 2015; Xue et al., 2015; Yang et al., 2017). Dimensionless Kuhn's anisotropic ratios in the ES and GS, being popularly known as g_{lum} and g_{abs} , were manually evaluated at a specific extreme wavelength (λ_{ext}) of the corresponding CPL and CD spectral profiles in line with the literature (Eliel and Wilen, 1994). All CPL characteristics (g_{lum} value at λ_{ext}) of Eu^{III} and Tb^{III} complexes are summarized in **Table 1**.

TABLE 1 | CPL characteristics (dissymmetry ratio, g_{lum} in 10^{-2} at specific wavelength) of Eu^{III} and Tb^{III} coordinated with three β -diketonates as achiral ligands embedded in two polysaccharide alkyl esters (**CABu** and **CTA**), *D*-/*L*-glucose pentamethyl esters (**D**-/**L**-**Glu**), and *D*-/*L*-Arabinose tetramethyl esters (**D**-/**L**-**Ara**).

Ln^{III} tris(β -diketonates)	CABu $g_{lum}/10^{-2}$ (nm)	CTA $g_{lum}/10^{-2}$ (nm)	Glu $g_{lum}/10^{-2}$ (nm)		Ara $g_{lum}/10^{-2}$ (nm)		α -pinene $g_{lum}/10^{-2}$ (nm)	
			<i>D</i> -	<i>L</i> -	<i>D</i> -	<i>L</i> -	(1R)	(1S)
$Eu(fod)_3$	+6.71 (593) ^a −0.59 (613) ^b	+4.63 (593) ^a −0.40 (613) ^b	+1.05 (594) ^a −0.19 (612) ^b	−0.81 (596) ^a +0.08 (613) ^b	+0.19 (593) ^a −0.02 (607) ^b	−0.30 (591) ^a +0.06 (611) ^b	−0.49 (593) ^f +0.05 (613) ^f	+0.41 (593) ^f −0.04 (613) ^f
$Eu(dpm)_3$	n.d. ^g	n.d. ^g	n.d. ^g	n.d. ^g	n.d. ^g	n.d. ^g	n.d. ^g	n.d. ^g
$Tb(fod)_3$	−0.29 (490) ^c +0.78 (540) ^d −0.18 (552) ^e	−0.10 (490) ^c +0.35 (542) ^d −0.07 (553) ^e	n.d. ^g	n.d. ^g				
$Tb(dpm)_3$	−0.53 (491) ^c +0.37 (537) ^d −0.59 (547) ^e	−0.44 (489) ^c − +0.80 (547) ^e	n.d. ^g	n.d. ^g	n.d. ^g	n.d. ^g	n.d. ^g (~490) +0.44 ^d (537) −0.13 ^e (547)	n.d. ^g (~490) −0.49 ^d (537) +0.34 ^e (548)

All numerical values in bracket mean wavelength extremum for CPL signals. ^a $Eu^{III} \ ^5D_0 \rightarrow \ ^7F_1$ (593 nm), ^b $Eu^{III} \ ^5D_0 \rightarrow \ ^7F_2$ (613 nm), ^c $Tb^{III} \ ^5D_4 \rightarrow \ ^7F_6$ (490 nm), ^d $Tb^{III} \ ^5D_4 \rightarrow \ ^7F_5$ (l) (540 nm), ^e $Tb^{III} \ ^5D_4 \rightarrow \ ^7F_5$ (ll) (552 nm), ^fData were taken from literature (Jalilah et al., 2018). ^gNot characterized or no data.

Chirality Transfer Capability From Cellulose Alkyl Esters to $Eu(fod)_3$

The normalized CD and UV-visible spectra of $Eu(fod)_3$ in **CABu** and **CTA** films are shown in **Figures 2A,B**, respectively. For comparison, the original raw CD and UV-visible spectra of the $Eu(fod)_3$ -hybridized films were given in **Figure S13A**, SM. Bisignate profile at Cotton CD bands at 290 and 310 nm between **CABu** and **CTA** films are obviously opposite. These Cotton CD bands at 290 and 310 nm, however, do not originate from **CABu** and **CTA**. Broad monosignate CD bands due to $n-\pi^*$ transition from alkyl esters of **CABu** and **CTA** thin films appeared at ~215 nm with (+)-sign and ~205 nm with (−)-sign, respectively (Guo et al., 2018). These (+)- and (−)-sign CD bands at 205 and 215 nm in the solid film reflect from left-handed helicity of **CABu** and right-handed helicity of **CTA** in solutions, respectively (Dubois et al., 1998; Onofrei et al., 2015), though **CABu** and **CTA** are β -(1 \rightarrow 4) linked polymers made of *D*-glucose framework as a common repeating unit.

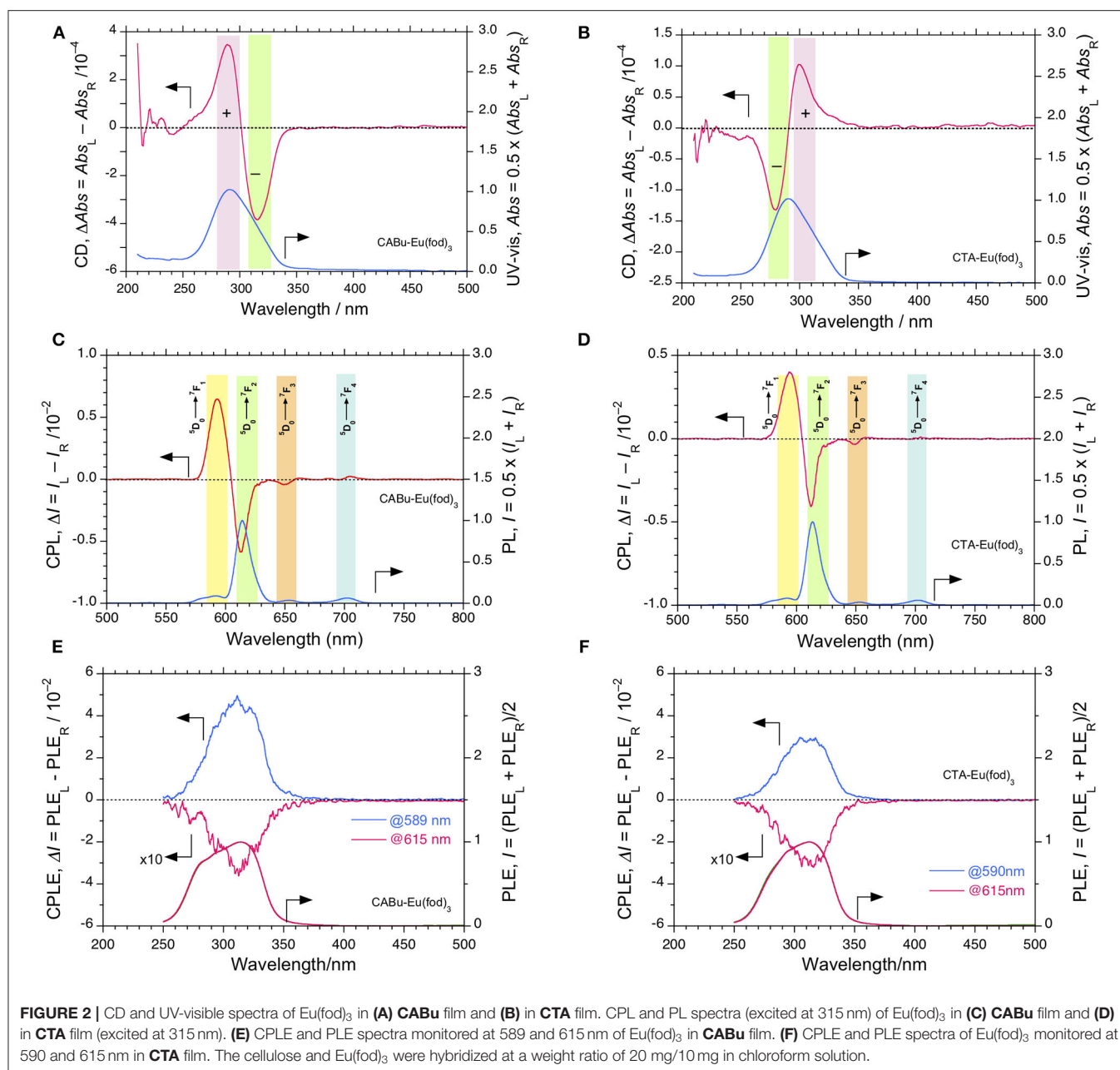
Although the alkyl ester itself does not have a stereogenic center, the ester can adopt particular chiral conformational geometry by the direct connection of the *D*-glucose ring. Two lone pairs at ethereal “−O−” and two C−H groups at “−CH₂−” are no longer to be equal because of C−O−C single bonds in R−C(=O)−O−CH₂− side group act as pseudochiral stereogenic bonds, similar to gauche *n*-butane. The unequal lone pairs at ethereal oxygen and unequal CH₂ groups may be responsible for the induction of chiral intermolecular C−O/H−C and C−H/F−C interactions between the alkyl ester moieties and lanthanide ligands. However, any CD/CPL signals of $Eu(fod)_3$ in the presence of **CABu** and **CTA** in dilute chloroform solutions (~10^{−3} M) were not able to detect because the postulated chiral intermolecular C−O/H−C and C−H/F−C interactions are inherently weak in the fluidic solution. The postulated chiral alkyl esters of **CABu** and **CTA** can thus act efficiently and differently in the solidified films only as external chirality

inducible scaffoldings toward optically inactive $Eu(fod)_3$ and several lanthanide complexes, as discussed in later sections.

The g_{abs} values at λ_{ext} of $Eu(fod)_3$ at 290 and 316 nm in **CABu** film are $+3.5 \times 10^{-4}$ at 280 nm and -3.5×10^{-4} at 310 nm, respectively, while those in **CTA** film are -1.6×10^{-4} at 290 nm and $+1.1 \times 10^{-4}$ at 300 nm, respectively. Note that the λ_{max} values at non-polarized UV-visible spectra of $Eu(fod)_3$ in **CABu** and **CTA** films are commonly ~291 nm. Although these CD bands at ~290 nm and ~310 nm are ascribed to $n-\pi^*/\pi-\pi^*$ bands of the three fod ligands, their signs appear to be determined solely by preferential helix sense and/or local chirality of multiple alkyl esters of **CABu** and **CTA**.

Contrarily, the normalized bisignate-like CPL spectral profiles between $Eu(fod)_3$ in **CABu** and **CTA** films are apparently the same, as shown in **Figures 2C,D**, respectively. Obviously, bisignate CPL band profiles at ~593 nm and ~613 nm in **CABu** and **CTA** are definitively similar. The g_{lum} values of $Eu(fod)_3$ in **CABu** film are $+6.71 \times 10^{-2}$ at $^5D_0 \rightarrow ^7F_1$ transition (593 nm) and -0.59×10^{-2} at $^5D_0 \rightarrow ^7F_2$ transition (613 nm), respectively, while those in **CTA** film are weaker with $+4.63 \times 10^{-2}$ at $^5D_0 \rightarrow ^7F_1$ transition (593 nm) and -0.40×10^{-2} at $^5D_0 \rightarrow ^7F_2$ transition (613 nm), respectively (**Table 1**).

It is interesting to note that the absolute magnitude $|g_{lum}|$ values at $^5D_0 \rightarrow ^7F_1$ band of $Eu(fod)_3$, 6.7×10^{-2} in **CABu** and 4.6×10^{-2} in **CTA** are considerably boosted by 13–16 times and 9–11 times, respectively, relative to the $|g_{lum}|$ values of $Eu(fod)_3$ in neat (*R*)- and (*S*)- α -pinene (Jalilah et al., 2018). Also, those $|g_{lum}|$ values are enhanced by 2.5–2.7 times and 1.7–1.9 times compared to those of $Eu(fod)_3$ in neat (*R*)- and (*S*)- α -phenylethylamine (Jalilah et al., 2018). Although the $|g_{lum}|$ values of $Eu(fod)_3$ in **CABu** and **CTA** are not outstanding compared to those several Eu^{III} complexes coordinated with well-designed chiral ligands reported recently (Petoud et al., 2007; Lunkley et al., 2008; Leonzio et al., 2017; Yeung et al., 2017; Zhou et al., 2019), the **CABu** and **CTA** have a tremendous benefit as chiral solidified platforms

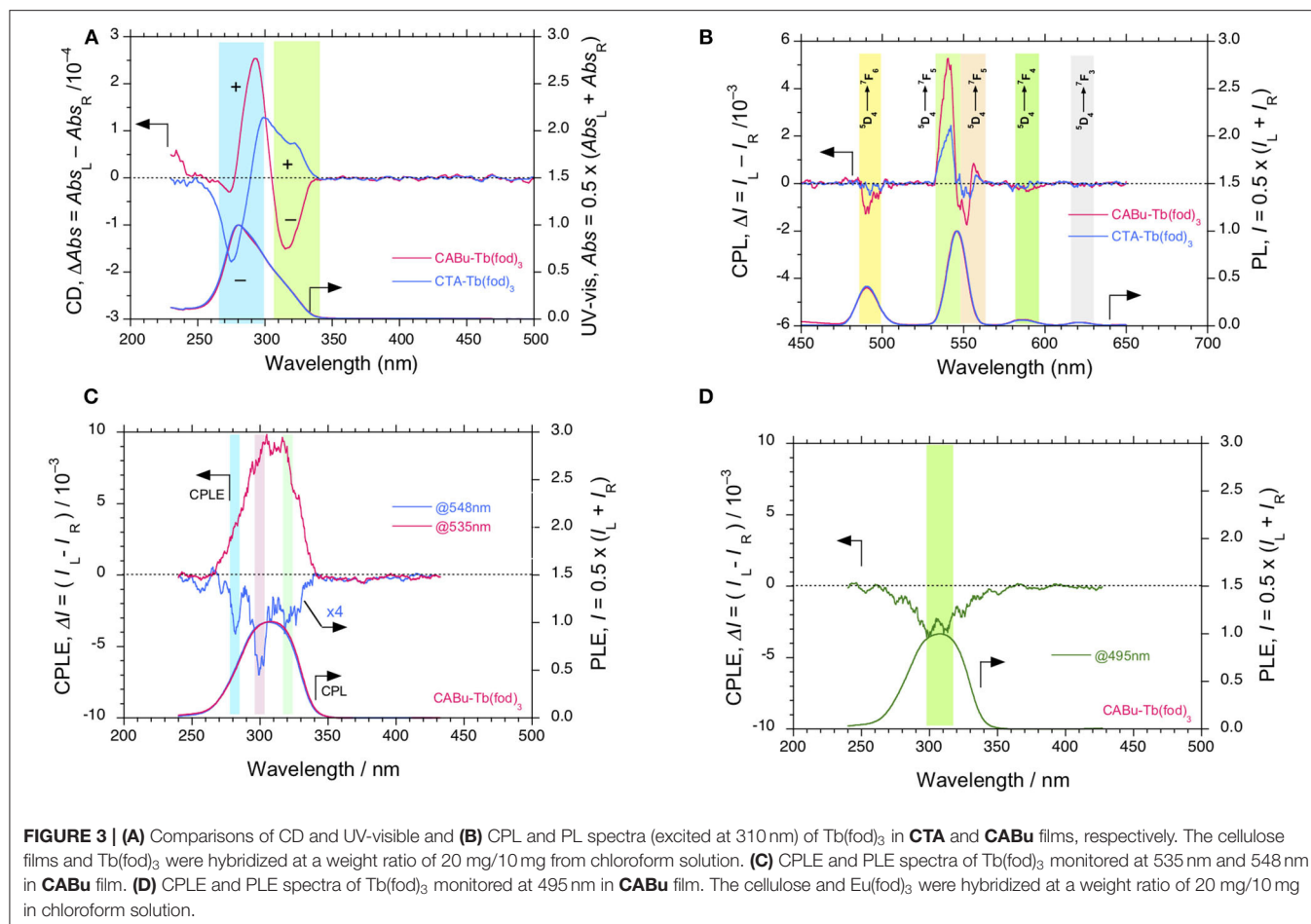


to efficiently induce and magnify $|g_{\text{lum}}|$ values to optically inactive $\text{Eu}(\text{fod})_3$ as a potent CPL emitter regardless of achiral ligands.

To confirm the apparent inconsistency between the retention in CPL bands at $4f-4f$ transitions in **CABu** and **CTA** films and between the inversion in CD bands at $n-\pi^1\pi-3\pi^*$ transitions in **CABu** and **CTA** films, we applied CPL and PLE spectroscopy (Duong and Fujiki, 2017) by monitoring at $^5\text{D}_0 \rightarrow ^7\text{F}_1$ and $^5\text{D}_0 \rightarrow ^7\text{F}_2$ transitions in **CABu** and **CTA** films, as shown in **Figures 2E,F**, respectively. Disregard of **CABu** and **CTA**, it is obvious that the CPL band at 310 nm is commonly (+)-sign monitored at $^5\text{D}_0 \rightarrow ^7\text{F}_1$ transition and that the CPL band at 310 nm is commonly (-)-sign monitored at $^5\text{D}_0 \rightarrow ^7\text{F}_2$

transition. The magnitudes of the CPL bands in **CABu** film are $+4.86 \times 10^{-2}$ monitored at 589 nm and -0.30×10^{-2} monitored at 615 nm, respectively. Similarly, the magnitude of the CPL bands in **CTA** film somewhat weaken, and $+2.96 \times 10^{-2}$ monitored at 590 nm and -0.33×10^{-2} monitored at 615 nm, respectively.

The origin of the inconsistency between the sign at the first Cotton CD band (310 nm) and the opposite CPL sign at this wavelength that depends on the wavelengths monitored at $^5\text{D}_0 \rightarrow ^7\text{F}_1$ and $^5\text{D}_0 \rightarrow ^7\text{F}_2$ transitions is an unresolved question and obscure. However, the $n-\pi^1\pi-3\pi^*$ bands at ~ 310 nm with the opposite sign originates from the three fod ligands, is obviously degenerative, and is responsible for LMCT (from the



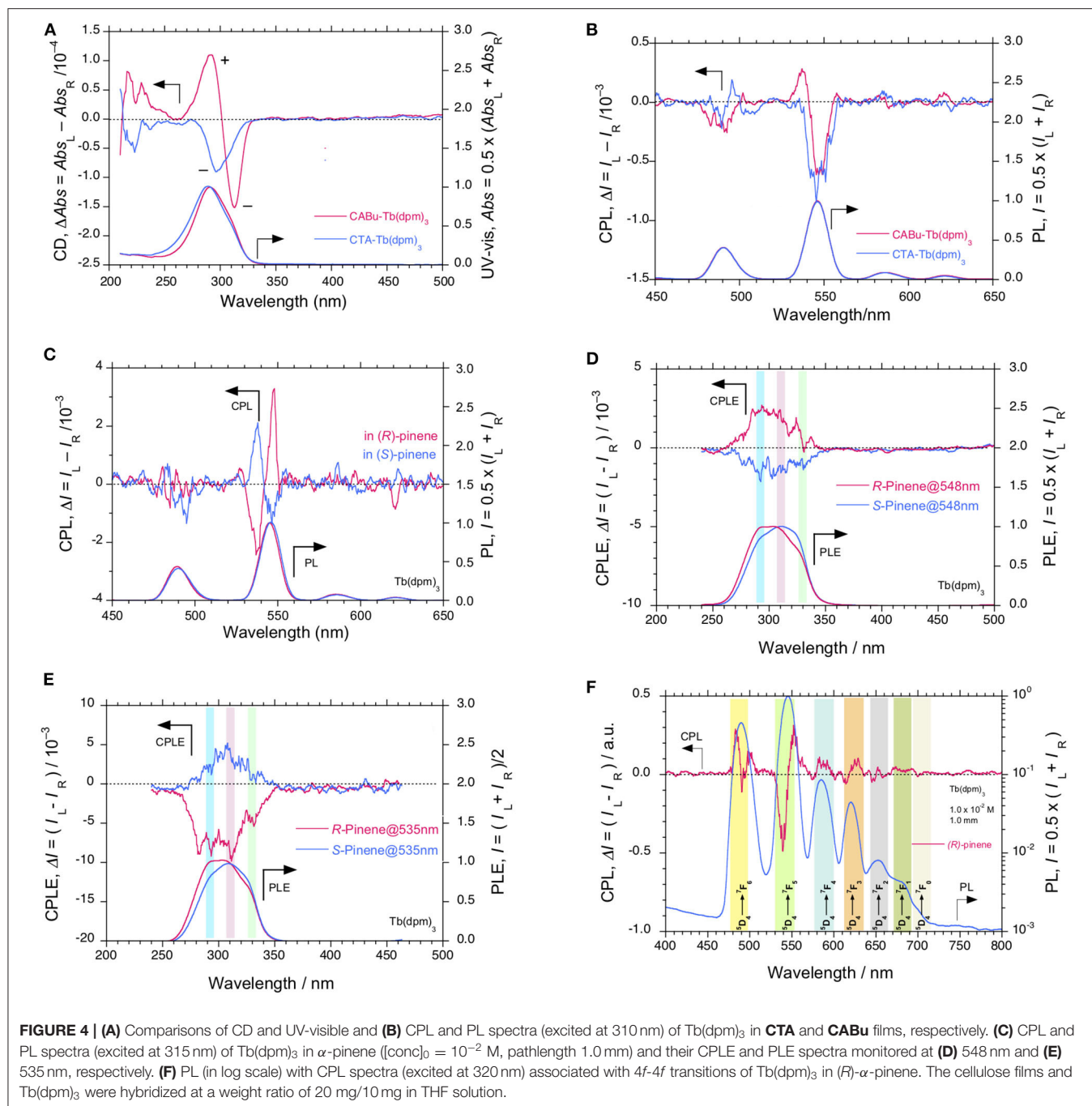
ligands to high energy levels of Eu^{III}, for example, ⁵D₂ state), leading to ⁵D₀ → ⁷F₁ and ⁵D₀ → ⁷F₂ transitions with the opposite CPL sign. The broader ~310 nm transition is likely to be a convolution of two nearly degenerate transitions with an opposite chirality; one (+)-sign band at ~310 nm is responsible for ⁵D₀ → ⁷F₁ and another (-)-sign band at ~310 nm for ⁵D₀ → ⁷F₂ bands. The ⁵D₂ state of Eu^{III} is close to the lowest photoexcited T₁ states of the ligands. When one excite simultaneously at couplet-like ¹π-³π* transitions (~310 nm) of CD-active Eu(fod)₃ using monochromated non-polarized light, the photoexcited Eu(fod)₃ decays into the ⁷F₁ and ⁷F₂ states with two different pathways because ⁵D₀ → ⁷F₁ and ⁵D₀ → ⁷F₂ states are magnetic dipole (MD) allowed transition with an electric dipole (ED) forbidden transition and MD forbidden transition with a forced induced ED transition, so-called, hypersensitive transition, respectively (Tanner, 2013; Binnemans, 2015).

Chirality Transfer Capability From Cellulose Alkyl Esters to Tb(fod)₃

The normalized CD and UV-visible spectra of Tb(fod)₃ in **CTA** and **CABu** films are compared in **Figure 3A**. For comparison, the original CD and UV-visible spectra of the films were given in **Figure S13B**, SM. Unlikely to the case of Eu(fod)₃, trisignate

profile at CD bands appeared at (-)-sign at 315 nm, (+)-sign at 292 nm and (-)-sign at 273 nm in **CABu** while (+)-sign at 322 nm, (+)-sign at 300 nm and (-)-sign at 275 nm in **CTA**. The apparent g_{abs} values at the first Cotton CD band of Tb(fod)₃ in **CABu** and **CTA** films are -3.5×10^{-4} at 315 nm and $+2.0 \times 10^{-4}$ at 324 nm, respectively. **CABu** efficiently induced the Cotton CD band of Tb(fod)₃ rather than **CTA**, similar to the case of Eu(fod)₃.

The different CD inducibility of Tb(fod)₃ between **CABu** and **CTA** reflects the corresponding CPL spectra at 4f-4f transitions of Tb(fod)₃. **Figure 3B** shows the normalized CPL and PL spectra excited at 310 nm of Tb(fod)₃ in **CTA** and **CABu** films. Obviously, three CPL bands are ascribed to ⁵D₄ → ⁷F₆ transition (490 nm) and ⁵D₄ → ⁷F₅ transitions (540 and 552 nm), respectively (**Table 1**). On the other hand, we did not detect any CPL bands at ⁵D₄ → ⁷F₄ transition (585 nm) and ⁵D₄ → ⁷F₃ transition (622 nm) clearly though the corresponding PL band was obvious. The g_{lum} values of Tb(fod)₃ in **CABu** are -2.91×10^{-3} at ⁵D₄ → ⁷F₆ transition (490 nm), $+7.82 \times 10^{-3}$ at ⁵D₄ → ⁷F₅ transition (540 nm) and -1.75×10^{-3} at ⁵D₄ → ⁷F₅ transition (552 nm), respectively (**Table 1**). Those values in **CTA** weaken with -1.01×10^{-3} at ⁵D₄ → ⁷F₆ transition (490 nm), $+3.53 \times 10^{-3}$ at ⁵D₄ → ⁷F₅ transition (542 nm) and -0.68×10^{-3} at ⁵D₄ → ⁷F₅ transition (553 nm), respectively (**Table 1**). Although the origin of the differences in the g_{abs} at



the first Cotton CD bands and g_{lum} values of CPL bands at 4f-4f transitions between Eu(fod)₃ and Tb(fod)₃ remains, CABu and CTA commonly induced clear CD and CPL bands.

Although the $|g_{lum}|$ values ($0.35\text{--}0.78 \times 10^{-2}$ at 540 nm, Table 1) at $^5D_4 \rightarrow ^7F_5$ transition of Tb(fod)₃ in CABu and CTA films are comparable to those (0.83×10^{-2} at 542 nm) of Tb^{III}(hfa)₃ (hfa:hexafluoroacetate) with chiral 4,12-bis(diphenylphosphino)-[2.2]-paracyclophane (Taniguchi et al., 2019) and weakened by one order of magnitude compared to those ($4\text{--}8 \times 10^{-2}$ at ~ 540 nm) of Tb^{III} complexes

coordinated with chiral bis(oxazolonyl)pyridine (Yuasa et al., 2011). The well-designed chiral ligands induce CPL-functionality to Tb^{III} complexes in solution more efficiently than solidified polysaccharide alkyl esters.

Chirality Transfer Capability From Cellulose Alkyl Esters to Eu(dpm)₃ and Tb(dpm)₃

The dpm ligand is a symmetrical β -diketonate, in which two methyl groups of acetylacetonate are replaced by two electron-donating (ED) *tert*-butyl groups. Therefore, Tb(dpm)₃ and

Eu(dpm)₃ can adopt a single *D*₃-symmetrical configuration (Brittain and Richardson, 1977a; Brittain, 1980). In a recent paper (Jalilah et al., 2018) and the present work, we confirmed that Eu(fod)₃ in α -pinene has shown clear CPL signals due to the presence of electron-withdrawing (EW) fluoroalkyl groups. Eu(dpm)₃ in α -pinene shows no detectable CPL signals due to the lack of EW fluoroalkyl groups (Figure S14B, SM).

Tb(dpm)₃ in CABu and CTA films shows clear CD and UV-visible spectra in the range of 200 nm and 340 nm, as shown in Figure 4A. For comparison, the original CD and UV-visible spectra of the films are given in Figure S13C, SM. Tb(dpm)₃ in CABu and CTA films, however, showed detectable but weak CPL spectra at 4*f*-4*f* transitions, as shown in Figure 4B. The *g*_{lum} values in CABu film are -0.53×10^{-3} at ⁵D₄ → ⁷F₆ (491 nm), $+0.37 \times 10^{-3}$ at ⁵D₄ → ⁷F₅ (537 nm), -0.59×10^{-3} at ⁵D₄ → ⁷F₅ (547 nm), while the *g*_{lum} values in CTA are -0.44×10^{-3} at ⁵D₄ → ⁷F₆ (489 nm) and -0.80×10^{-3} at ⁵D₄ → ⁷F₅ (547 nm) (Table 1). The absolute magnitudes of *g*_{lum} values with dpm ligands greatly diminished compared to Tb^{III} complexes with fod ligands. Tb(dpm)₃ and Eu(dpm)₃ showed different behaviors toward external chiral chemical perturbations regardless of the same fod and dpm as the ligands. Eu(dpm)₃ in CABu and CTA did not demonstrate obvious CPL spectra although the corresponding PL spectra are evident (Figures S14A,B, SM).

We ascertained many times that there were no detectable CPL signals of Eu(dpm)₃ in CABu films. This could be because Eu(dpm)₃ is lack of EW-fluoroalkyl groups that can cause efficient chiral C-F/H-C interactions. Chiral C-O/H-C interactions seem not efficient to induce the chiral perturbation.

Chirality Transfer Capability From Monosaccharide Permethyl Esters to Eu(fod)₃ and Tb(fod)₃

Kipping and Pope found that preferential crystallization of *L*-NaClO₃ in the presence of naturally occurring *D*-glucose and *D*-mannitol (Kipping and Pope, 1898). Currently, non-naturally occurring *L*-glucose is available commercially, although it is costly. *L*-(+)- and *D*-(-)-arabinose are also available, but the *L*-form is more abundant in nature than the *D*-form due to unknown reasons. To verify whether chirogenesis of Eu(fod)₃ is solely determined by point chirality of monosaccharides, we measured CD and CPL spectra of Eu(fod)₃ embedded in *D*-/*L*-Glu and *D*-/*L*-Ara films, as displayed in Figures 5A-D.

Firstly, CD and UV-visible spectra between Eu(fod)₃ in *D*- and *L*-Glu films are compared in Figure 5A. The original CD and UV-visible spectra of the films are given in Figure S13D, SM. Eu(fod)₃ showed nearly mirror-image bisignate CD bands, though the value of λ_{ext} at the first and second Cotton bands are considerably different from each other. The *g*_{abs} values of Eu(fod)₃ in *D*-Glu film are $+0.89 \times 10^{-4}$ at 321 nm and -0.42×10^{-4} at 284 nm, while in *L*-Glu film, these values are -0.80×10^{-4} at 315 nm and $+0.44 \times 10^{-4}$ at 282 nm (Table 1).

CD and UV-visible spectra between Eu(fod)₃ in *D*- and *L*-Ara films are compared in Figure 5B. The original CD and UV-visible spectra of the films are given in Figure S13E, SM. Similarly, Eu(fod)₃ shows nearly mirror-image bisignate CD bands, though

the value of λ_{ext} at the first and second Cotton bands are subtly different. The *g*_{abs} values of Eu(fod)₃ in *D*-Ara are -0.96×10^{-4} at 321 nm and $+0.55 \times 10^{-4}$ at 281 nm, respectively, while in *L*-Glu film, these values are $+1.08 \times 10^{-4}$ at 316 nm and -0.39×10^{-4} at 275 nm, respectively (Table 1).

Next, we compared CPL and PL spectra excited at 315 nm of Eu(fod)₃ in *D*- and *L*-Glu films, shown in Figure 5C. Eu(fod)₃ displays nearly mirror-image trisignate CPL bands at 4*f*-4*f* transitions associated with emission wavelengths, though the absolute *g*_{lum} values at these transitions are somewhat different. The *g*_{lum} values in *D*-Glu are $+1.05 \times 10^{-2}$ at ⁵D₀ → ⁷F₁ (594 nm), -0.19×10^{-2} at ⁵D₀ → ⁷F₂ (612 nm) and $+0.19 \times 10^{-2}$ at ⁵D₀ → ⁷F₂ (626 nm), while in *L*-Glu, these values are -0.81×10^{-2} at ⁵D₀ → ⁷F₁ (596 nm), $+0.08 \times 10^{-2}$ at ⁵D₀ → ⁷F₂ (613 nm), and -0.04×10^{-2} at ⁵D₀ → ⁷F₂ (627 nm) (Table 1).

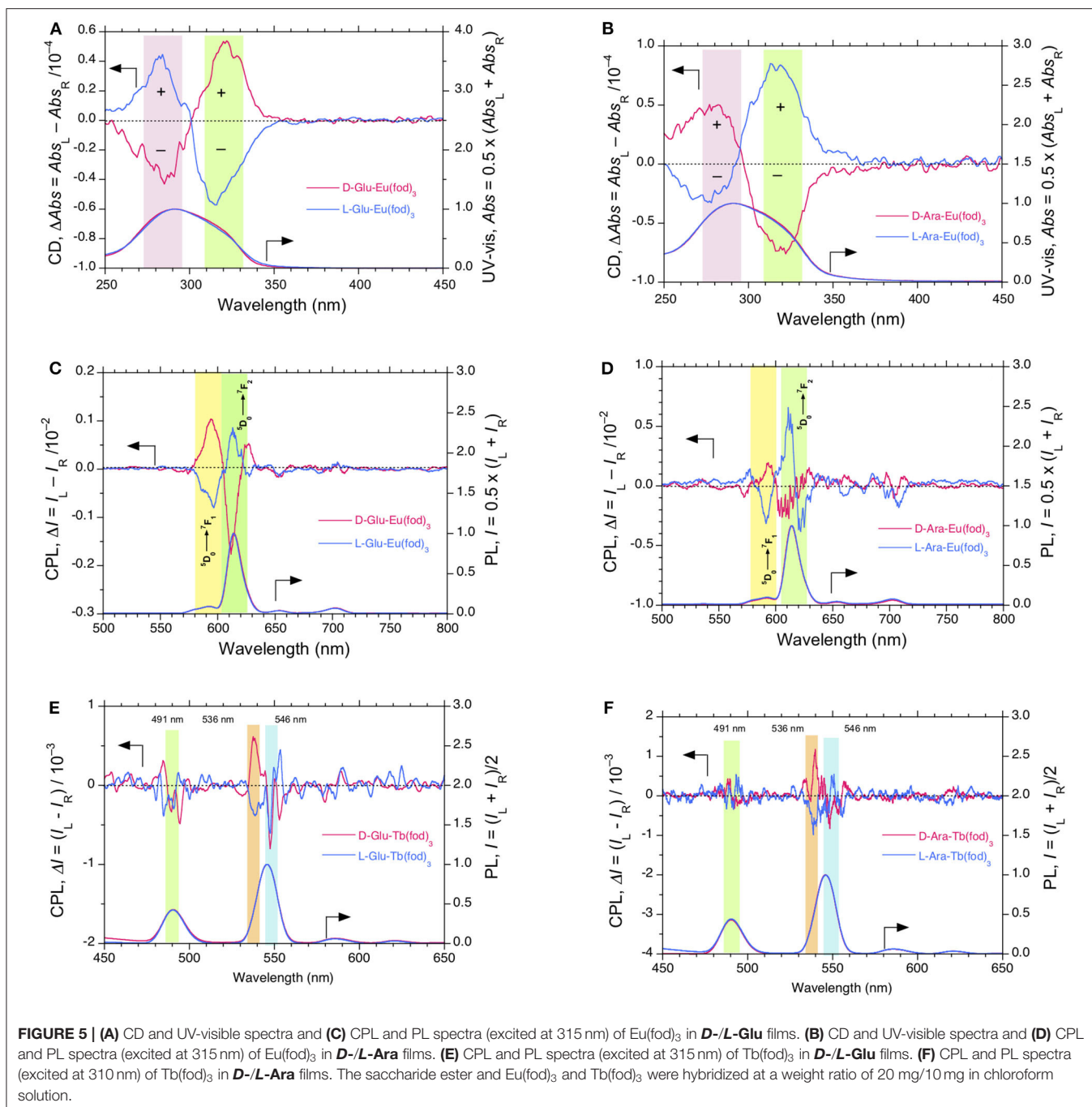
For comparison, CPL and PL spectra of Eu(fod)₃ in *D*- and *L*-Ara films were excited at 315 nm, and the results are presented in Figure 5D. Eu(fod)₃ exhibits no longer mirror-image trisignate CPL bands at 4*f*-4*f* transitions, though the absolute *g*_{lum} values at these transitions weaken several times. The *g*_{lum} values in *D*-Ara are $+0.19 \times 10^{-2}$ at ⁵D₀ → ⁷F₁ (593 nm), -0.02×10^{-2} at ⁵D₀ → ⁷F₂ (607 nm), and $+0.42 \times 10^{-2}$ at ⁵D₀ → ⁷F₂ (630 nm), while in *L*-Ara, these values are -0.30×10^{-2} at ⁵D₀ → ⁷F₁ (591 nm), $+0.06 \times 10^{-2}$ at ⁵D₀ → ⁷F₂ (611 nm), and -0.72×10^{-2} at ⁵D₀ → ⁷F₂ (622 nm) (Table 1).

CPL and PL spectra of Tb(fod)₃ excited at 315 nm in *D*-/*L*-Glu and *D*-/*L*-Ara films are given in Figures 5E,F, respectively. Regardless of Glu and Ara, although Tb(fod)₃ shows very weak CPL bands at 4*f*-4*f* transitions, CPL signs are likely to depend on the chirality of Glu and Ara. Because the absolute *g*_{lum} values at these 4*f*-4*f* transitions considerably weaken, the *g*_{lum} values cannot be precisely evaluated.

Although *L*-cellulose is not available on earth, we can conclude that *D*-chirality of CTA, CABu, Glu, and Ara determines the (+)- and (-)-sign CPL characteristics of Eu(fod)₃ at ⁵D₀ → ⁷F₁ and ⁵D₀ → ⁷F₂ transitions. Conversely, (-)- and (+)-signs at these transitions are from the *L*-chirality of Glu and Ara, although the inversion in the bisignate CD bands of Eu(fod)₃ at 280–290 nm and 300–310 nm are considerably dependent on the nature of the alkyl groups of CTA and CABu. Similarly, *D*-chirality of CTA, CABu, Glu, and Ara determines the (+)- and (-)-sign CPL characteristics of Tb(fod)₃ at two ⁵D₄ → ⁷F₅ transitions. Conversely, *L*-chirality of Glu and Ara determines the (-)- and (+)-signs at the transitions.

Chirality Transfer Capability From α -Pinene to Eu(fod)₃, Tb(fod)₃, Eu(dpm)₃, and Tb(dpm)₃

Bicyclic terpenes, (1*S*)-/(1*R*)- α -pinene and (1*S*)-/(1*R*)- β -pinene, are chiral rigid hydrocarbons and are transparent in the near-UV and visible region. This feature is beneficial to gain an insight into higher energy states responsible for CPL transitions by measuring CPLE spectra monitoring at a specific CPL wavelength. Actually, the chirality of α -/ β -pinenes is transferred to achiral or racemic Eu(fod)₃ with considerably large *g*_{lum} values at 4*f*-4*f* transitions,



that were verified by CPLE spectra (Jalilah et al., 2018). This result prompted us to test whether $\text{Tb}(\text{fod})_3$ in α -pinene reveals CPL signals, although $\text{Tb}(\text{fod})_3$ did not show clear CPL signals because of an unknown reason.

On the other hand, $\text{Tb}(\text{dpm})_3$ dissolved in α -pinene shows clear CPL signals, in which signs are determined solely by the chirality of the α -pinene (Figure 4C). The g_{lum} values in (1*S*)- α -pinene are $+4.35 \times 10^{-3}$ at $^5\text{D}_4 \rightarrow ^7\text{F}_5$ (537 nm) and -1.28×10^{-3} at $^5\text{D}_4 \rightarrow ^7\text{F}_5$ (547 nm), while in (1*R*)- α -pinene are -4.94×10^{-3} at $^5\text{D}_4 \rightarrow ^7\text{F}_5$ (537 nm) and $+3.44 \times 10^{-3}$ at

$^5\text{D}_4 \rightarrow ^7\text{F}_5$ (548 nm), though the CPL bands at $^5\text{D}_4 \rightarrow ^7\text{F}_6$ (490 nm) are not obvious (Table 1). Evidently, (+), (-) and (-) sign CPL characteristics of $\text{Eu}(\text{fod})_3$ at $^5\text{D}_0 \rightarrow ^7\text{F}_1/5\text{D}_0 \rightarrow ^7\text{F}_2$ transitions and $\text{Tb}(\text{dpm})_3$ at two $^5\text{D}_4 \rightarrow ^7\text{F}_5$ transitions are determined by *S*- and *R*-chirality of α -pinene, respectively. In comparison to $\text{Tb}(\text{dpm})_3$, $\text{Eu}(\text{dpm})_3$ in α -pinene has shown no detectable CPL signals (Figure S14C, SM). From PL spectrum of $\text{Tb}(\text{dpm})_3$ in (*R*)- α -pinene excited at 320 nm associated with the corresponding CPL signals ranging of 500 and 800 nm (Figure 4F), seven characteristic *4f*-*4f* transitions were assigned

to ${}^5D_4 \rightarrow {}^7F_6$ (490.0 nm, 20408 cm^{-1}), ${}^5D_4 \rightarrow {}^7F_5$ (545.5 nm, 18330 cm^{-1}), ${}^5D_4 \rightarrow {}^7F_4$ (584.5 nm, 17,109 cm^{-1}), ${}^5D_4 \rightarrow {}^7F_3$ (620.0 nm, 16129 cm^{-1}), ${}^5D_4 \rightarrow {}^7F_2$ (652.5 nm, 15,326 cm^{-1}), ${}^5D_4 \rightarrow {}^7F_1$ (682.0 nm, 14,663 cm^{-1}), and ${}^5D_4 \rightarrow {}^7F_0$ (702.5 nm, 14,235 cm^{-1}) (Fulgêncio et al., 2012; de Queiroz et al., 2015; Xue et al., 2015; Yang et al., 2017).

We further verified these CPL signals of $\text{Tb}(\text{dpm})_3$ by the broad CPLE spectra centered at ~ 300 nm associated with the corresponding PLE spectra with several shoulders, as marked by blue, pink, and green bars in **Figures 4D,E**. The signs of the CPLE spectra depend on the signs at monitor wavelengths (535 and 548 nm) and α -pinene chirality; (+)-sign in CPLE spectrum is identical to (+)-sign CPL signal at 546 nm in (*R*)-pinene, while (+)-sign in CPLE spectrum is the same of (+)-sign CPL signal at 535 nm in (*S*)-pinene. The broad CPLE/PLE spectra may arise from at least three different origins of $n\text{-}\pi^*/{}^1\pi\text{-}3\pi^*$ transitions of three dpm ligands associated with high energy levels (e.g., 5D_1 and 5D_2) of Tb^{III} (Fulgêncio et al., 2012; de Queiroz et al., 2015; Xue et al., 2015). A similar tendency can be seen in the broad CPLE/PLE spectra of $\text{Tb}(\text{fod})_3$ in **CABu**, as marked in blue, pink, and green bars in **Figures 3C,D**.

Unresolved factors between Tb^{III} and Eu^{III} associated with ligands (fod and dpm) and chiral matrices (α -pinene and monosaccharide alkyl esters) are other critical parameters to generate CPL signals and boost g_{lum} characteristics. Although the inherent nature of the differences between Tb^{III} and Eu^{III} is unresolved, we assume that the interactions of $C\text{-}H/\pi$ between $C(\delta\text{-})\text{-}H(\delta\text{+})$ bonds at dpm of $\text{Tb}(\text{dpm})_3$ and $C(\delta\text{+})\text{-}C(\delta\text{-})$ double bond of α -pinene are more crucial while the $C\text{-}F/H\text{-}C$ interactions between $C(\delta\text{+})\text{-}F(\delta\text{-})$ bonds of fod ligands and $H(\delta\text{+})\text{-}C(\delta\text{-})$ bonds of α -pinene are crucial (Jalilah et al., 2018).

Intermolecular Interactions Between $\text{Eu}(\text{fod})_3$ and **CTA/Glu** by Solid-State ${}^{13}\text{C}\{^1\text{H}\}$ -NMR and Solution ${}^1\text{H}/{}^{19}\text{F}$ -NMR Spectra

We do not yet know what kinds of intermolecular noncovalent interactions exist between the lanthanide tris(β -diketonate) and the poly-/monosaccharide alkyl esters. Among lanthanide tris(β -diketonate)s, we chose $\text{Eu}(\text{fod})_3$ for simplicity and excellent solubility in CDCl_3 . The three fod ligands have ${}^1\text{H}$, ${}^{19}\text{F}$, and ${}^{13}\text{C}$ -NMR active elements to discuss the possible interactions. Additionally, we chose **CTA** and ***D*-/*L*-Glu** for simplicity in these solid-state (*ss*)- ${}^{13}\text{C}$ -NMR and solution ${}^1\text{H}$ -/ ${}^{19}\text{F}$ -NMR spectra. According to the hard-soft-acid-base theory proposed by Pearson (Pearson, 1963), the lone pairs of the hard base O atom(s) of ester groups can coordinate with the hard acid Eu^{III} of $\text{Eu}(\text{fod})_3$. A marked chemical shift in ${}^{13}\text{C}$ -NMR spectra of ester ($\text{C}=\text{O}$ and O) and ethereal $\text{C}\text{-O}\text{-C}$ atoms was expected.

The *ss*- ${}^{13}\text{C}\{^1\text{H}\}$ -NMR spectra of $\text{Eu}(\text{fod})_3$, **CTA**, and a mixture of $\text{Eu}(\text{fod})_3$ and **CTA** in 1/1 (w/w) are compared in **Figures 6A,B**. The *ss*- ${}^{13}\text{C}$ -NMR spectra of the $\text{Eu}(\text{fod})_3\text{-CTA}$ mixture are merely a convolution of those of **CTA** and $\text{Eu}(\text{fod})_3$. Any noticeable chemical shift in the ${}^{13}\text{C}$ -NMR spectra was not seen. ${}^{13}\text{C}$ -NMR chemical shift at ~ 170 ppm due to $\text{O}=\text{C}\text{-O}$ of **CTA** was unchanged after mixing with $\text{Eu}(\text{fod})_3$.

The *ss*- ${}^{13}\text{C}\{^1\text{H}\}$ -NMR spectra of $\text{Eu}(\text{fod})_3$, ***D*-Glu**, and a mixture of $\text{Eu}(\text{fod})_3$ and ***D*-Glu** in 1/1 (w/w) are compared in **Figures 6C–G**. Similarly, the *ss*- ${}^{13}\text{C}$ -NMR spectra of the $\text{Eu}(\text{fod})_3\text{-D-Glu}$ mixture are merely a convolution of those of ***D*-Glu** and $\text{Eu}(\text{fod})_3$. Any remarkable chemical shift in the ${}^{13}\text{C}$ -NMR spectra was not seen. Even five well-resolved $\text{O}=\text{C}\text{-O}$ peaks of ***D*-Glu** pentamethyl ester ranging of ~ 169 ppm and ~ 173 ppm showed no detectable chemical shifts (**Figure 6D**). Similarly, no noticeable chemical shifts of three well-resolved methyl groups ranging from ~ 19 ppm to ~ 22 ppm were observed (**Figure 6E**). Among five well-resolved ${}^{13}\text{C}$ peaks assignable to $\text{O}=\text{C}\text{-O}$ of five esters, $\text{C}\text{-O}\text{-C}$ pyranose ring ranging from ~ 64 to ~ 72 ppm and at ~ 83 ppm does not show remarkable chemical shifts of *D*-glucose ring. These *ss*- ${}^{13}\text{C}\{^1\text{H}\}$ -NMR data led us to the conclusion that any O atom(s) of glucose ring and ester moieties do not coordinate directly to Eu^{III} ions.

On the other hand, alterations in the chemical shifts of the solution ${}^{19}\text{F}$ -NMR spectra of $\text{Eu}(\text{fod})_3$ in the absence and presence of **CTA**, ***D*-Glu**, and ***L*-Glu** in CDCl_3 are apparent, as shown in **Figures 7A–C**. The outer CF_3 signal of $\text{Eu}(\text{fod})_3$ in CDCl_3 resonates at -81.73 ppm as a single peak, indicating C_3 -symmetrical geometry (**Figure 7B**). The single peak resonates at -82.21 ppm and -82.26 ppm in the absence and presence of ***L*-Glu** and ***D*-Glu**, respectively, and shifts upfield by 0.48 ppm and 0.53 ppm, respectively (**Figure 7B**). In the presence of **CTA**, the CF_3 signal resonates at -82.31 ppm and shifts upfield by 0.58 ppm (**Figure 7B**). Although the middle CF_2 signal of fod ligand resonates broadly at -126 ppm, in the presence of ***L*-Glu** and ***D*-Glu**, this signal resonates at -127.4 ppm and -127.5 ppm, that is shifted upfield by 1.4 ppm and 1.5 ppm, respectively (**Figure 7C**). Similarly, the middle CF_2 peak at -127.5 ppm shifts upfield by 1.5 ppm in the presence of **CTA** (**Figure 7C**). The inner CF_2 of fod shows a broad resonance at -129.2 ppm, but this signal appears at -130.1 ppm in the presence of ***L*-** and ***D*-Glu** and shifts upfield by 0.9 ppm (**Figure 7C**). Similarly, the signal appears at -130.3 ppm in the presence of **CTA** and shifts upfield by 1.1 ppm. These upfield shifts in the ${}^{19}\text{F}$ -NMR spectra indicate intermolecular interactions between the F atoms and **CTA**, ***L*-Glu**, and ***D*-Glu**, possibly, $\text{C}\text{-}F(\delta\text{-})$ (of the three fod ligands)/ $H(\delta\text{+})\text{-}C$ (of **CTA** and **Glu**) interactions.

It is thus evident that there were no marked alterations in *ss*- ${}^{13}\text{C}$ -NMR spectra between CPL-inactive and CPL-active $\text{Eu}(\text{fod})_3$ in **CTA**, ***L*-Glu**, and ***D*-Glu**, while the remarkable upfield chemical shifts in ${}^{19}\text{F}$ -NMR of fod ligands in dilute CDCl_3 solution was distinct. These characteristics should arise from outer or second-sphere effects perturbed by chiral chemicals that are non-coordinating to Eu^{III} , the so-called 'Pfeiffer effect'. The multiple $H(\delta\text{+})\text{-}C(\delta\text{-})$ bonds of chiral chemical species (**CTA**, ***D*-/*L*-Glu**, possibly, ***D*-/*L*-Ara** and **CABu**) interact with multiple $F(\delta\text{-})\text{-}C(\delta\text{+})$ bonds of the three fod ligands but do not directly coordinate with Eu^{III} .

The noticeable downfield chemical shifts in ${}^1\text{H}$ -NMR spectra of ***D*-Glu** and **CTA** support the postulated $\text{C}(\delta\text{+})\text{-}F(\delta\text{-})$ (of fod) and $H(\delta\text{+})\text{-}C(\delta\text{-})$ (of **CTA** and ***D*-/*L*-Glu**) interaction. **Figure 8A** displays the changes in ${}^1\text{H}$ -NMR spectra of ***D*-Glu** in the absence and presence of $\text{Eu}(\text{fod})_3$. All protons are assigned in the inset of the Figure. The degree of the downfield shifts is summarized

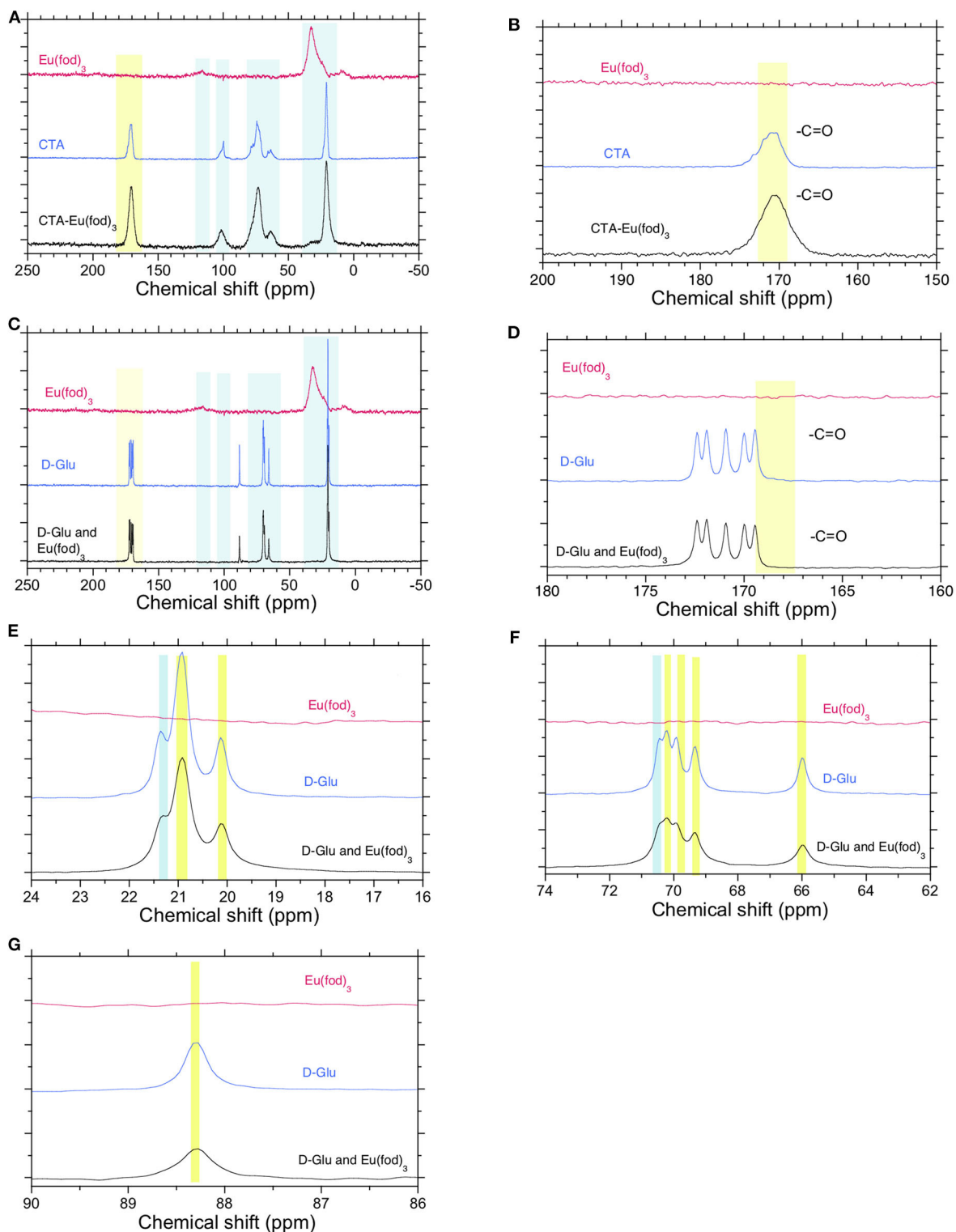
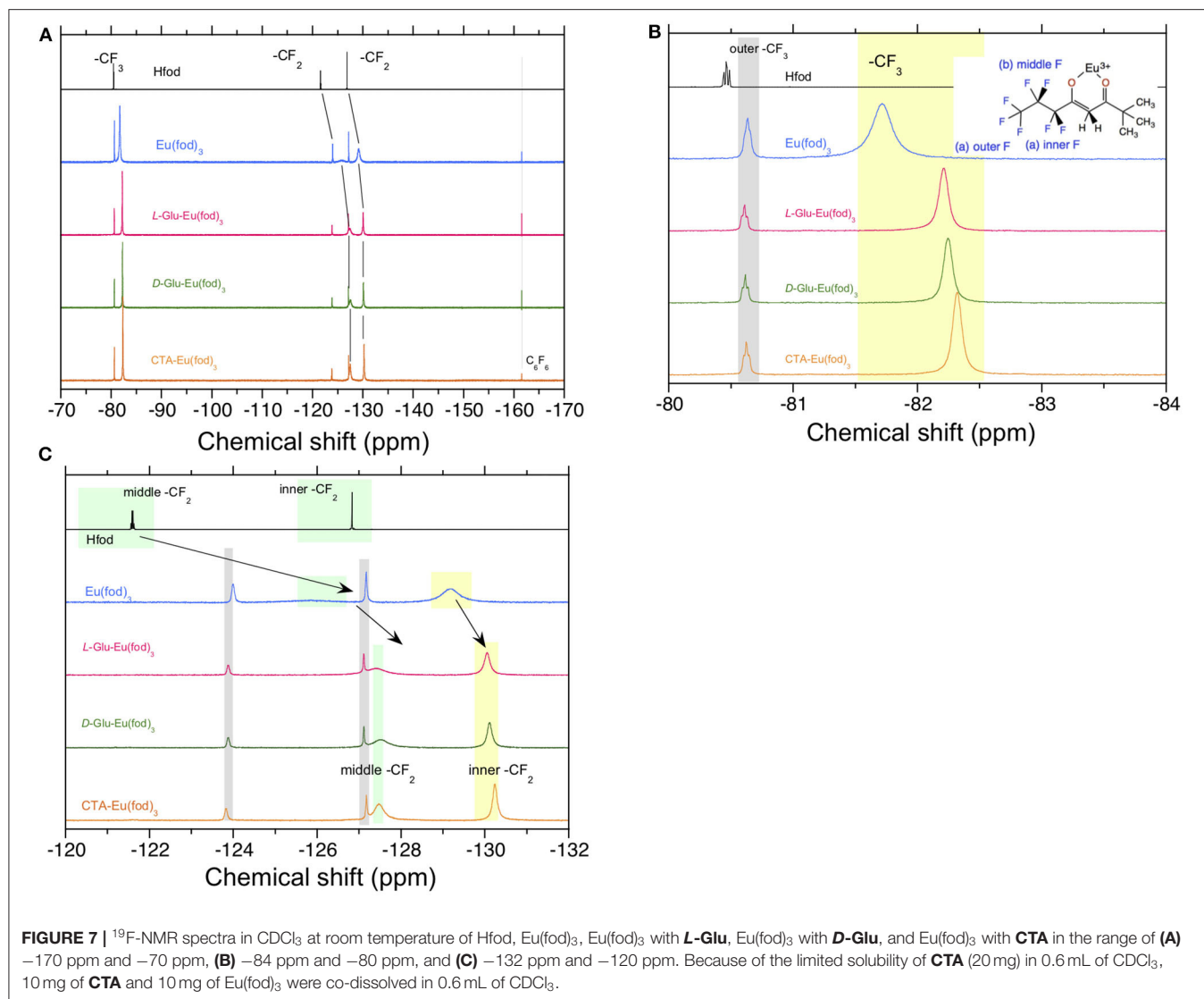


FIGURE 6 | (A) Solid-state (ss)-CP/MAS- $^{13}\text{C}\{^1\text{H}\}$ -NMR spectra of $\text{Eu}(\text{fod})_3$, **CTA**, and a mixture of $\text{Eu}(\text{fod})_3$ and **CTA** in 1/1 (w/w). **(B)** Its magnified spectrum in the range of 150–200 ppm. **(C)** ss- $^{13}\text{C}\{^1\text{H}\}$ -NMR spectra of $\text{Eu}(\text{fod})_3$, **D-Glu**, and a mixture of $\text{Eu}(\text{fod})_3$ and **D-Glu** in 1/1 (w/w) **(D,E)**. Their magnified spectra of methyl groups in **D-Glu** in the range of 150–200 ppm and 16–24 ppm **(F,G)**. Their magnified spectra of **D**-glucose ring in the range of 62–90 ppm. A broad ^{13}C -NMR signal at 130 ppm (Figures 5A,C) was attributable to β -diketonate.



in **Table 2**. Notably, protons H1, H3, H5, H6 shift downfield significantly and protons H2, H4, H6 (one of two), H7 also considerably shift downfield. We noticed that H1, H3, H5 are the glucose ring protons and H6 is the CH_2 attached to C5 carbon. Possibly, $\text{Eu}(\text{fod})_3$ molecule is placed on top of the *D*-glucose ring. All H1–H7 protons are close to $\text{Eu}(\text{fod})_3$ molecule with the help of multiple $\text{C}(\delta^+)-\text{F}(\delta^-)/\text{H}(\delta^+)-\text{C}(\delta^-)$ and $\text{C}(\delta^-)-\text{H}(\delta^+)/\text{O}(\delta^-)-\text{C}(\delta^+)$ interactions.

Figure 8B exhibits similar changes in ^1H -NMR spectra of **CTA** in the absence and presence of $\text{Eu}(\text{fod})_3$. Protons are assigned in the insets of the figure. The degree of downfield shifts is summarized in **Table 2**. Notably, protons H1 and H2 shift downfield greatly and protons H3, H4, H5 also shift considerably downfield. H1, H2, H3, and H4 are the glucose ring protons and H5 is the CH_2 attached to C4 carbon. Similarly, $\text{Eu}(\text{fod})_3$ molecule is placed on top of the *D*-glucose ring of **CTA**. All H1–H5 protons are close to $\text{Eu}(\text{fod})_3$ molecule with the

help of multiple $\text{C}(\delta^+)-\text{F}(\delta^-)/\text{H}(\delta^+)-\text{C}(\delta^-)$ and $\text{C}(\delta^-)-\text{H}(\delta^+)/\text{O}(\delta^-)-\text{C}(\delta^+)$ interactions.

For comparison, FT-IR spectra between $\text{Eu}(\text{fod})_3$, **D-Glu**, and $\text{Eu}(\text{fod})_3$ mixed with **D-Glu** in the ranges of 2,700 and 3,700 cm^{-1} , 2,800 and 3,100 cm^{-1} , and 1,000 and 2,000 cm^{-1} are shown in **Figures S15A–C**, SM. We observed no noticeable frequency shifts in $\nu(\text{C-H})$ at 2,850–3,000 cm^{-1} and $\nu(\text{C-F})$ at 1,250–1,050 cm^{-1} . Since the postulated $\text{C-F}/\text{H-C}$ and $\text{C-H}/\text{O-C}$ interactions are very weak, the resulting frequency shifts might be minimal, possibly, within 10 cm^{-1} . One $\nu^{\text{as}}(\text{C-H})$ at 2973 cm^{-1} and $\nu^{\text{s}}(\text{C-H})$ at 2873 cm^{-1} due to methyl groups of fod in the absence of **D-Glu** shift to lower frequencies at 2967 cm^{-1} by 7 cm^{-1} and 2871 by 2 cm^{-1} , respectively (**Figure S15B**, SM). These small shifts may be the consequence of the $\text{C-H}/\text{O-C}$ interactions. On the other hand, $\nu(\text{C=O})$ at $\sim 1,750$ cm^{-1} characteristic of five ester group of **D-Glu** does not coordinate to Eu^{III} directly because there are no noticeable frequency shifts (**Figure S15C**,

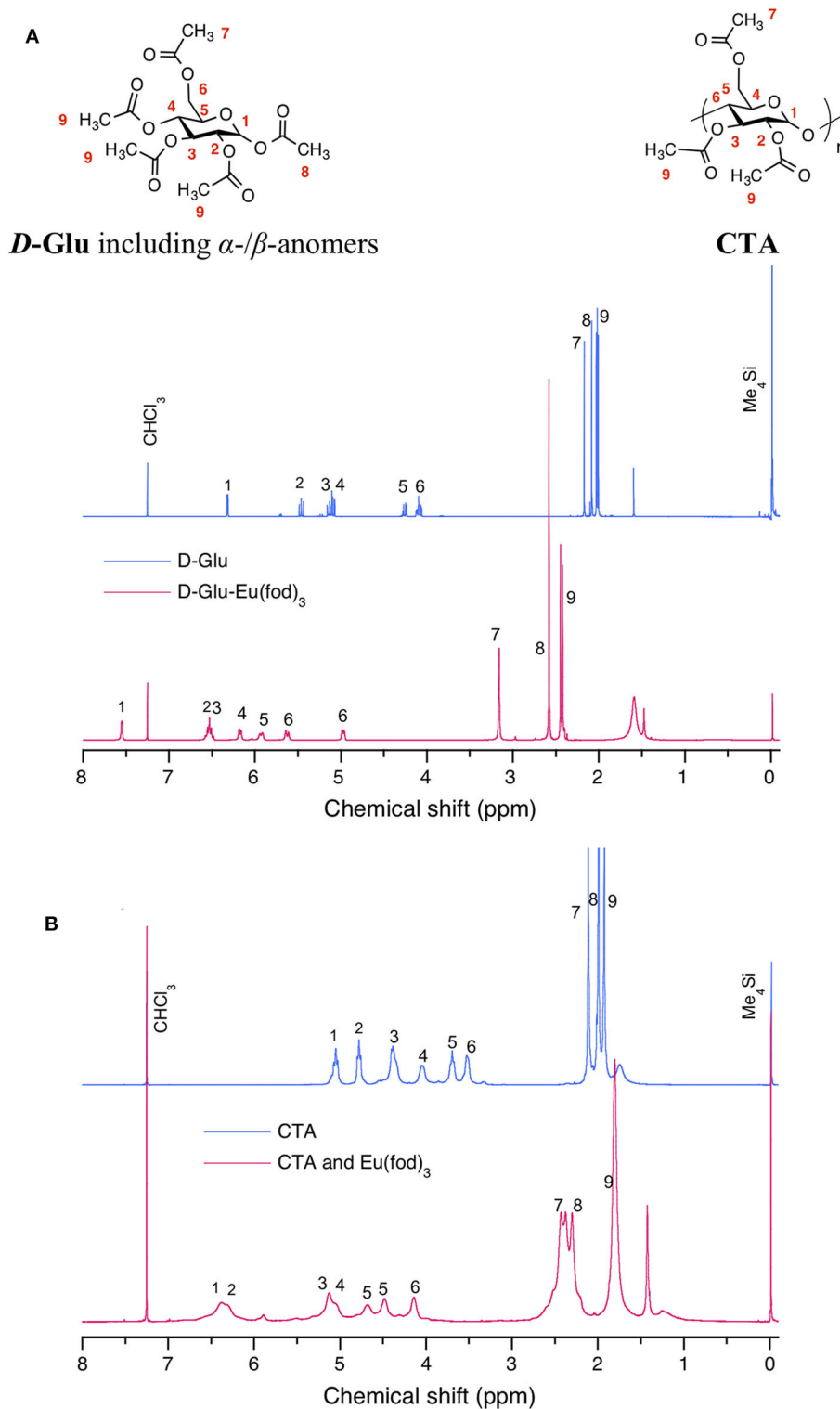


FIGURE 8 | Comparison of ¹H-NMR spectra in CDCl₃ at room temperature between **(A)** *D-Glu* (blue) and Eu(fod)₃ with *D-Glu* (red) and between **(B)** *CTA* (blue) and Eu(fod)₃ with *CTA* (red). Sharper and broader ¹H-NMR peaks at ~1.5 ppm are assumed to be free water in CDCl₃ and bounded waters at Eu(fod)₃, respectively. Although 20 mg of *D-Glu* and 10 mg of Eu(fod)₃ were able to co-dissolve in 0.6 mL of CDCl₃, 10 mg of *CTA* and 10 mg of Eu(fod)₃ were co-dissolved in 0.6 mL of CDCl₃ because of the limited solubility of 20 mg *CTA* in 0.6 ml of CDCl₃.

TABLE 2 | Comparison of chemical shifts in the $^1\text{H-NMR}$ spectra in CDCl_3 at room temperature between (a) *D-Glu* without and with $\text{Eu}(\text{fod})_3$ and between (b) CTA without and with $\text{Eu}(\text{fod})_3$, whereas (+)-sign stands for the downfield shift.

	1	2	3	4	5	6	7	8	9
<i>D-Glu</i>	6.31	5.45	5.14	5.09	4.26	4.09	2.17	2.08	2.01
$\text{Eu}(\text{fod})_3$ in <i>D-Glu</i>	7.55	6.53	6.53	6.17	5.93	5.61, 4.99	3.16	2.58	2.44, 2.42
Relative shifts of $^1\text{H-NMR}$	+1.24	+1.08	+1.39	+1.08	+1.67	+1.52, +0.90	+0.99	+0.50	+0.41, +0.43
CTA	5.05	4.78	4.37	4.04	3.70	3.52	2.10	1.99	1.92
$\text{Eu}(\text{fod})_3$ in CTA	6.38	6.31	5.12	5.05	4.67, 4.49	4.13	2.40	2.31	1.81
Relative shifts of $^1\text{H-NMR}$	+1.33	+1.53	+0.75	+1.01	+0.93, +0.79	+0.61	+0.30	+0.32	-0.11

TABLE 3 | Lifetimes of photoexcited $\text{Eu}(\text{fod})_3$, $\text{Eu}(\text{dpm})_3$, and $\text{Tb}(\text{dpm})_3$ embedded to CTA and CABu films^a.

Lanthanide complexes	$\text{Eu}(\text{dpm})_3$		$\text{Eu}(\text{fod})_3$		$\text{Tb}(\text{dpm})_3$	
	CTA	CABu	CTA	CABu	CTA	CABu
Poly(<i>D</i> -saccharide)s						
τ in msec	0.24 ^b	0.29 ^b	0.44 ^b	0.50 ^b	0.59 ^c	0.92 ^c

^aPulsed N_2 laser, 337.1 nm, 10 Hz repetition, Grating 150 lines per mm, slit width 100 μm .

^bAt room temperature, detected at 615 nm (collected from 610 to 620 nm), ^cdetected at 546 nm (collected from 542 to 551 nm).

SM). Although, in the absence of *D-Glu*, $\text{Eu}(\text{fod})_3$ has one broad and one shoulder $\nu(\text{C}=\text{O})$ band at 1621 cm^{-1} and 1594 cm^{-1} due to the β -diketonate, in the presence of *D-Glu*, the shoulder $\nu(\text{C}=\text{O})$ may disappear and merge to 1621 cm^{-1} or shift to 1642 cm^{-1} due to specific alteration of β -diketonates. Other frequency shifts such as $\nu(\text{C}-\text{O}-\text{C})$ at $\sim 1200\text{ cm}^{-1}$ and 1150 cm^{-1} of the ester groups and glucose rings of *D-Glu* are not apparent because of significant overlapping with other intense $\nu(\text{C}-\text{F})$ bands. The *C-F/H-C* interactions are not obvious due to the significant overlapping.

Figures S16A–C, SM compare the FT-IR spectra between $\text{Eu}(\text{fod})_3$, CABu, and $\text{Eu}(\text{fod})_3$ with CABu in the ranges of $2,700$ and $3,700\text{ cm}^{-1}$, $2,800$ and $3,100\text{ cm}^{-1}$, and $1,000$ and $2,000\text{ cm}^{-1}$. Similarly, minimal frequency shifts in $\nu(\text{C}-\text{H})$ at $2,850$ – $3,000\text{ cm}^{-1}$ can be seen due to the postulated *C-F/H-C* and *C-H/O-C* interactions (**Figure S16B**, SM). The $\nu^{\text{as}}(\text{C}-\text{H})$ band at $2,973\text{ cm}^{-1}$ and $\nu^{\text{s}}(\text{C}-\text{H})$ at $2,873\text{ cm}^{-1}$ of fod methyl groups in the absence of CABu shift to lower frequencies at $2,967\text{ cm}^{-1}$ by 7 cm^{-1} and conversely higher frequency of $2,878\text{ cm}^{-1}$ by 5 cm^{-1} , respectively (**Figure S16B**, SM). These small shifts may arise from the *C-H/O-C* interactions. On the other hand, a broad $\nu(\text{C}=\text{O})$ band at $\sim 1,630\text{ cm}^{-1}$ characteristic of the β -diketonate split into two $\nu(\text{C}=\text{O})$ bands at $1,643\text{ cm}^{-1}$ and $1,623\text{ cm}^{-1}$, suggesting specific structural alterations of the β -diketonates by the ester groups and/or ethers of CABu. However, no noticeable frequency shifts of $\nu(\text{C}-\text{O}-\text{C})$ at $\sim 1,200\text{ cm}^{-1}$ and $1,150\text{ cm}^{-1}$ of the ester groups of CABu are not seen because of the spectral overlapping with the intense $\nu(\text{C}-\text{F})$ bands (**Figure S16C**, SM).

Photodynamics of $\text{Eu}(\text{fod})_3$, $\text{Eu}(\text{dpm})_3$, and $\text{Tb}(\text{dpm})_3$ in CTA and CABu Films

Lifetimes of $\text{Eu}(\text{fod})_3$, $\text{Eu}(\text{dpm})_3$, and $\text{Tb}(\text{dpm})_3$ species embedded to CTA and CABu films excited at an N_2 pulsed

laser 337.1 nm are summarized in **Table 3** based on decay curves (semilog and linear plots) of these emitters (**Figures S17A–K**, SM). The decay times (τ) of these emitters in CABu are somewhat long by the magnitude of 15–56 % compared to those in CTA. Possibly, these emitters have differently interacted with CTA and CABu, that depends on the nature of alkyl esters. Alternatively, regardless of CTA and CABu, the values of τ belong to in the order of $\text{Eu}(\text{fod})_3$, $\text{Eu}(\text{dpm})_3$, and $\text{Tb}(\text{dpm})_3$, depending on the nature of lanthanides and ligands.

Mulliken Charges of Sc^{III} Tris(β -diketonate) as Models of Eu^{III} / Tb^{III} Tris(β -diketonate), *D-Glu* and *D-Glu* Dimer as a Model of CTA Obtained With MP2 (6-311G) Calculation

To theoretically discuss possible intermolecular interactions, we calculated Mulliken charges (Mulliken, 1955) by the Møller–Plesset second-order perturbation theory (MP2) (Møller and Plesset, 1934; Head-Gordon et al., 1988) (6-311G basis set) method of the model compounds optimized by MM (UFF force field), followed by DFT [6-31G(d)] methods (Frisch et al., 2013). Time-consuming MP2 calculation allows for reliable Mulliken charges compared to DFT calculation. **Figure 9** and **Figure S18**, SM display the numbering for all the atoms in the *D-Glu* and *D-Glu* dimer as a model of CTA. All the peripheral hydrogen atoms of *D-Glu* and *D-Glu* dimer show positive Mulliken charges ranging from $+0.215$ to $+0.261$. The $\text{O}=\text{C}$ atoms of methyl esters have substantial negative Mulliken charges of -0.464 . We observed that the $\text{O}-\text{C}$ atoms of methyl esters and the $\text{C}-\text{O}-\text{C}$ atom in pyranose rings and $\text{C}-\text{O}-\text{C}$ linkage between two pyranose rings show more substantial negative Mulliken charges ranging from -0.652 to -0.690 , respectively. When $\text{C}(\delta^-)-\text{H}(\delta^+)$ bond of the ligands (fod and dpm) feels the force

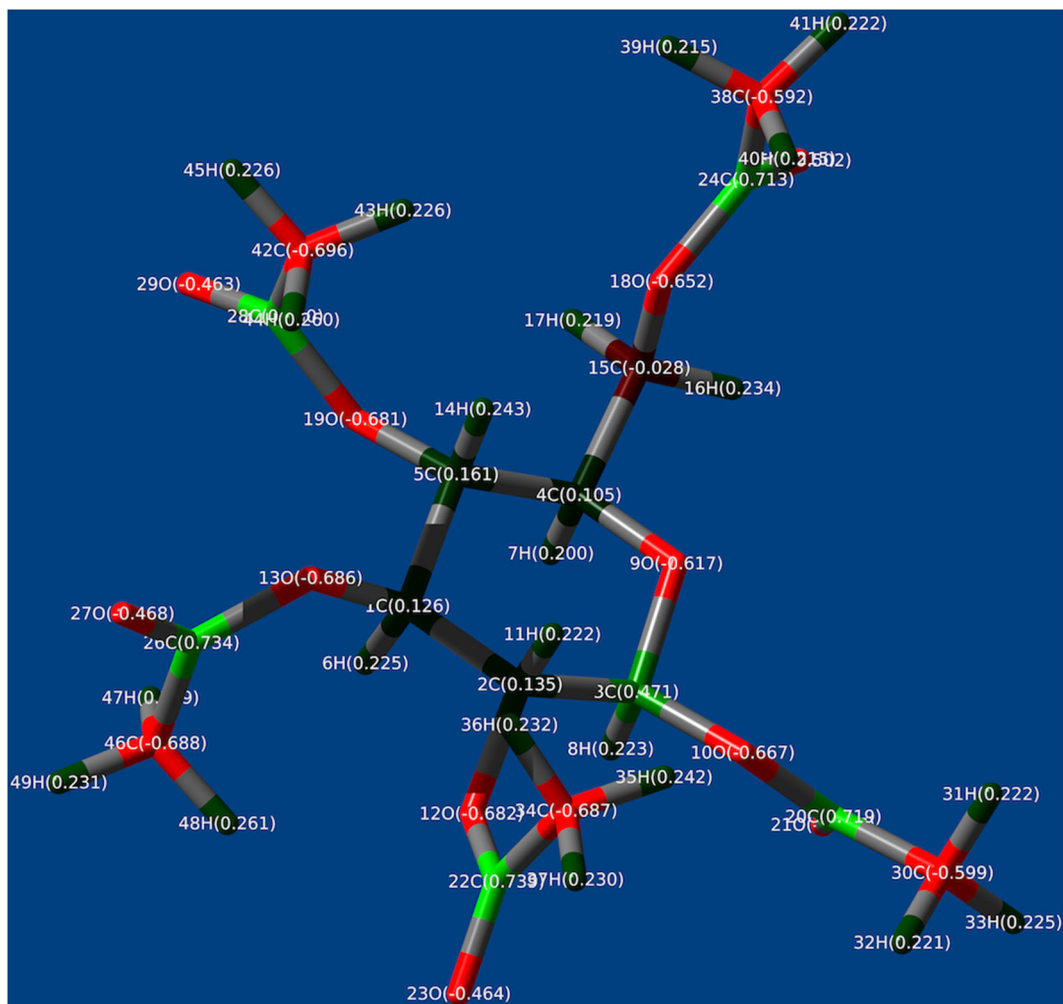


FIGURE 9 | The Mulliken charges of **D-Glu** obtained with MP2 (6-311 G basis set).

of oxygen atoms, the $C(\delta^+)-O(\delta^-)-C(\delta^+)$ and $C(\delta^+)-O(\delta^-)-C(\delta^+)=O(\delta^-)$ bonds are more crucial than $O(\delta^-)=C(\delta^+)$ bond of esters, leading to (ligand, $C-H$)/ O (**D-Glu**, possibly, **CTA**, **CABu**, **Glu**, and **Ara**) interactions.

In the previous paper (Jalilah et al., 2018), we proposed that the surplus charge neutralization obtained with Mulliken charges is a driving force of attractive forces between several ligands in the lanthanide complexes and CPL-inducible chiral substances. The fluorine atoms of $Sc(\text{fod})_3$ have negative Mulliken charges ranging from -0.341 to -0.373 ; conversely, the hydrogen atoms of $Sc(\text{fod})_3$ and $Sc(\text{dpm})_3$ have positive Mulliken charges ranging from $+0.153$ to $+0.193$.

The Mulliken charge neutralization between multiple (δ^-) fluorines of fod and multiple (δ^+) hydrogens of **D-Glu** and the saccharides is possible. Total surplus charge between $C(\delta^+)-F(\delta^-)$ (fod) and $H(\delta^+)-C(\delta^-)$ (saccharides, in this work) is that $3 \times (-0.35)$ (F_3C) + $(4\sim 5) \times (+0.20 \sim +0.24)$ (H_3C or H_2C) = $-0.05 \sim -0.09$. Additionally, the Mulliken charge neutralization between multiple (δ^+) hydrogens of the ligands

(fod and dpm) and multiple (δ^-) oxygen atoms of the saccharides are possible. Total surplus charge between (δ^-) $H(\delta^+)$ and $O(\delta^-)-C(\delta^+)$ (saccharides) is that $(4) \times (+0.17)$ ($H-C$) + $(1) \times (-0.62 \sim -0.69)$ ($O-C$ or $O-C=O$) = $+0.06 \sim -0.01$. Moreover, total surplus charge between (dpm and fod) $C(\delta^-)-H(\delta^+)$ and $C(\delta^-)=C(\delta^+)$ (α -pinene) is that $(1) \times (+0.17)$ ($H-C$) + $(1) \times (-0.18)$ ($C=C$) = -0.01 ; $Tb(\text{dpm})_3$ is a dominant factor, while $Eu(\text{dpm})_3$ is unimportant. However, it is reasonably assumed that the same Mulliken charges between multiple (δ^+) hydrogen atoms of ligands (fod and dpm) and multiple (δ^+) hydrogen atoms of the saccharides should cause repulsive interactions.

The Degree of Chirogenesis and the Pfeiffer Effects

Since the serendipitous finding by an anomaly in an optical rotation of chiral substances in the presence of optically inactive labile metal ions in aqueous solutions (Pfeiffer and Quehl, 1931, 1932), the chirogenesis in the GS and ES from

optically inactive labile metal complexes induced by chiral additives has been often appeared in the titles of several papers in the past and currently: e.g., Pfeiffer effect (Kirschner and Ahmad, 1968; Mayer and Brasted, 1973; Schipper, 1978; Brittain, 1982, 1984; Kirschner and Bakkar, 1982; Lunkley et al., 2018); outer-sphere coordination and complexation (Mason and Norman, 1965; Madaras and Brittain, 1980; Kirschner and Bakkar, 1982); second-sphere coordination (Colquhoun et al., 1986). Pfeiffer effect and/or outer-sphere/second-sphere coordination are mainly investigated in their solution states of the metal complexes.

An equilibrium shift from dynamic racemic mixtures ($\Delta:A = 50/50$) of labile metal complexes is responsible for the Pfeiffer effect and chirogenesis by outer-sphere/second-sphere coordination. A barrier height of racemization should be rather small to permit dynamic racemization at ambient temperatures. In 1975, Schipper theoretically discussed chemical discrimination between racemic substances (A' and A'') and chiral substance B surrounded by achiral solvent (Schipper, 1975) as a model of the Pfeiffer effect. In the hypothetical system, an exothermic enthalpic gain Δ_h/T is acquired to compensate an entropic loss Δ_s . The long-range interactions in dynamically dissociate system is needed to overcome thermal fluctuation $k_B T$.

To quantitatively discuss the degree of chirogenesis in six-coordinate labile lanthanide tris(β -diketonate) led by chiral additives in solution, we compare four solution PL spectra of $\text{Eu}(\text{fod})_3$ itself (10 mg, 0.8×10^{-2} M, red line) and in the presence of **D-Glu** (20 mg, 4×10^{-2} M, blue line), **L-Glu** (20 mg, 4×10^{-2} M, green line), and **CTA** (10 mg, 3×10^{-2} M, black line) in 1.2 mL of CDCl_3 (Figure S19, SM). These CDCl_3 solutions were used prior to measurements of ^{19}F - and ^1H -NMR spectra (Figure 7). Among $^5\text{D}_0$ - $^5\text{F}_J$ ($J = 0,1,2,3,4$) transitions, $^5\text{D}_0$ - $^5\text{F}_1$ transition at 594 nm is known to be susceptible to alterations in molecular symmetry and geometry coordinated with external ligands. Our previous investigation suggests that $\text{Eu}(\text{fod})_3$ is likely to adopt a facial C_3 -symmetrical structure and exists as a mixture of labile Δ - and Λ -isomers in solutions (Jalilah et al., 2018). Similar Pfeiffer effect was reported for D_3 -symmetrical labile $\text{TbIII}(\text{dpa})_3$ in the absence and presence of *L*-histidine, revealing no significant alteration in PL and CPL spectral profiles at 7F_5 - 5D_4 transition (Wu et al., 1989).

From Figure S19A in SM, we can see minimal alterations in magnitudes, wavelengths, and profiles in PL bands of $\text{Eu}(\text{fod})_3$ (non-chiral additive (red line), **D-Glu** (blue line), **L-Glu** (green line), and **CTA** (black line) at the five $^5\text{D}_0$ - $^5\text{F}_J$ ($J = 0,1,2,3,4$) transitions. Any apparent change in PL wavelength (593.0 nm) of $\text{Eu}(\text{fod})_3$ (non-chiral additive, **D-Glu**, **L-Glu**) is not detectable, while subtle changes in wavelength and magnitude in PL spectra of $\text{Eu}(\text{fod})_3$ (non-chiral (593.0 nm) and **CTA** (592.0 nm)) is discernable. Clearly, PL intensity at $^5\text{D}_0$ - $^5\text{F}_0$ transition (580 nm) of non-chiral additive $\text{Eu}(\text{fod})_3$ increases in the presence of chiral additive in the order of **L-Glu** < **D-Glu** < **CTA**. Similar alterations in subtle increases and subtle spectral shifts at $^5\text{D}_0$ - $^5\text{F}_J$ ($J = 2,3,4$) transitions between $\text{Eu}(\text{fod})_3$ (non-chiral additive, **D-Glu**, **L-Glu**, and **CTA**) is observable (Figures S19C–E), SM). We thus conclude that C_3 -symmetrical $\text{Eu}(\text{fod})_3$ in CDCl_3 (0.8

$\times 10^{-2}$ M) maintains in the presence of **L-Glu**, **D-Glu**, **CTA** (3 – 4×10^{-2} M, 4–5-folds excess relative to $\text{Eu}(\text{fod})_3$).

To confirm the dynamic equilibrium shift of the Δ - Λ isomers, we compare CPL and PL spectra of (a) $\text{Eu}(\text{fod})_3$ (0.8×10^{-2} M, 10 mg) and **CTA** (3×10^{-2} M, 20 mg) in 1.2 mL of CDCl_3 (red line) and (b) thin solid films of $\text{Eu}(\text{fod})_3$ (10 mg, $\sim 5 \times 10^{-1}$ M) in **CTA** (20 mg) annealed at 100 °C in a vacuum overnight (blue line).

Previously, a simple thermodynamic analysis confirmed that the binding constant K_b using g_{lum} value at $^5\text{D}_0$ - $^5\text{F}_1$ transition between $\text{Eu}(\text{fod})_3$ and rigid chiral hydrocarbon, α -pinene, was on the order of 10^{-3} M^{-1} ; $0.7 \times 10^{-3} \text{ M}^{-1}$ for (1S)- α -pinene and $1.0 \times 10^{-3} \text{ M}^{-1}$ for (1R)- α -pinene (Jalilah et al., 2018). When a solvent quantity of α -pinene was used, even minimal K_b value was characterized as g_{lum} by CPL spectroscopy.

When a similar analysis was applied to $\text{Eu}(\text{fod})_3$ and non-rigid chiral **CTA**, we obtained $K_b = 0.09 \text{ M}^{-1}$ (Figures S21A,B), SM). This K_b value is more significant than that of α -pinene by two orders of magnitude and it is reasonable because a chiral repeating unit in **CTA** (though non-rigid and floppy) contains five oxygen atoms with the substantial (-)-Mulliken charges responsible for multiple pseudo chiral O/H–C interactions with achiral ligands (Figure 9 and Figure S18, SM). When solidified film and high concentrations of **CTA** were employed as chirality inducible scaffolds and platforms, the degree of chirogenesis was characterizable as g_{lum} values from CPL spectral characteristics. This idea can be extended to **CABu** and other four monosaccharide alkyl esters (Table 1).

CONCLUSION

Two polysaccharide alkyl esters (**CTA** and **CABu**) as the films, two enantiopairs of monosaccharide permethyl esters (**D-/L-Glu** and **D-/L-Ara**) as the films, and (1S)-/(1R)- α -pinene in solution were capable of transferring their chirality to several optically inactive Eu^{III} and Tb^{III} tris(β -diketonate) (= fod and dpm), which impart the shining CPL characteristics at $4f$ - $4f$ transitions. The greatest g_{lum} values at $^5\text{D}_0 \rightarrow ^7\text{F}_1$ transitions ($\lambda_{\text{ex}} = 315 \text{ nm}$) of $\text{Eu}(\text{fod})_3$ in **CABu** and **CTA** films are +0.067 and +0.046, respectively. $\text{Tb}(\text{fod})_3$ in **CABu** and **CTA** exhibited moderately large g_{lum} values of +0.008 and +0.004 at $^5\text{D}_4 \rightarrow ^7\text{F}_5$ transitions ($\lambda_{\text{ex}} = 315 \text{ nm}$), respectively. Meanwhile, **D-/L-Glu** and **D-/L-Ara** films induced weaker g_{lum} values for $\text{Eu}(\text{fod})_3$, $\text{Tb}(\text{fod})_3$, and $\text{Tb}(\text{dpm})_3$. **CTA** and **CABu** induced CPL signals more efficiently for $\text{Eu}(\text{fod})_3$ than **D-/L-Glu** and **D-/L-Ara**. Noticeably, the chirality of α -pinene enabled $\text{Tb}(\text{dpm})_3$ to shine similar CPL characteristics of $\text{Tb}(\text{fod})_3$ in **CABu**. However, $\text{Eu}(\text{dpm})_3$ in **CABu** films and α -pinene did not reveal CPL. From the analyses of solution ^1H -/ ^{19}F -NMR, solid-state ^{13}C -NMR with the help of MP2 (6–311G basis set) calculation, we propose that the surplus charge neutralization evaluated by the opposite Mulliken charges between $H(\delta+)$ - $C(\delta-)$ bonds of the poly- and monosaccharides and $F(\delta-)$ - $C(\delta+)$ bonds of the fluorinated ligands are the attractive driving forces to induce the CPL characteristics of $\text{Tb}(\text{fod})_3$ and $\text{Eu}(\text{fod})_3$. The present knowledge should enable the

fabrication of films, sheets, fibers, and nanocomposites that emit Eu^{III}-origin red-color and Tb^{III}-origin green-color CPL spectra with narrow spectral bandwidths. As demonstrated, Eu^{III}(fod)₃ and Tb^{III}(dpm)₃ containing transparent CTA films deposited on the Tempax substrate displayed clear Eu^{III}-origin red-color and Tb^{III}-origin green-color emissions upon 365-nm excitation (see, photographs in **Figure S22**, SM). These materials were obtainable by a chiral ligand-free process at room temperature by co-mixing soluble polysaccharide derivatives (and bacterial cellulose) and several optically inactive Eu^{III}/Tb^{III} complexes. The challenging issue remains to boost the rather small g_{lum} values [Eu(fod)₃: 6×10^{-2} at 593 nm and Tb(fod)₃: 0.8×10^{-2} at 540 nm] toward an ultimate $g_{\text{lum}} = \pm 2.0$, i.e., obtaining purely left- or right-CPL forms (Eliel and Wilen, 1994). Symmetry-oriented designing of emitters should be considered by precisely controlling topological shape associated with an efficient lens and an optofluidic effect (Wang et al., 2007; Di Pietro and Di Bari, 2012; Kruk et al., 2014; Khorasaninejad et al., 2016; Yeung et al., 2017; Tanaka et al., 2018; Zhou et al., 2019). A deeper understanding of the Pfeiffer effect in the GS and ES, magnetic dipole transitions of Eu^{III} and Tb^{III} complexes, colloidal aggregations, hybridization by other chromophores/luminophores, chain-like polymers, supramolecular motifs and polymers, and nature of oligo- and polysaccharides with conformational freedom are the next challenges (Wormald et al., 2002; Zou et al., 2019) in addition to several approaches to elaborate CPL and CD functions as polymeric colloids, revealing moderately high $|g_{\text{lum}}|$ and $|g_{\text{abs}}|$ values ($>10^{-2}$ - 10^{-1}) in the range of 300 and 800 nm (Nakano and Fujiki, 2011; Duong and Fujiki, 2017; Fujiki and Yoshimoto, 2017; Wang et al., 2017).

However, our approaches of chirogenesis from optically inactive labile Ln^{III} tris(β -diketonate) (Ln: lanthanide) induced by soluble chiral biomaterials is very limited to common organic solvents of Ln^{III} complexes and biomaterials. If water-soluble optically inactive labile Ln^{III} complexes are designed in the future, our approaches are applicable as a thin film state to sense and detect various water-soluble chiral substances including biomaterials, drug, medicine, pesticide, and virus consisting of illness-causing single-strand (ss)/double-strand (ds) RNA.

DATA AVAILABILITY STATEMENT

The raw data supporting the conclusions of this article will be made available by the authors, without undue reservation. Requests for the original CPL/CPL/CD/UV-visible/NMR/IR spectral and photodynamic data sets, followed by the processed data (#.qpc with #.qda and #.txt) using KaleidaGraph (mac, ver 4.53), and the calculation results (#.com, #.log, and #.chk up to 20 GB) of Gaussian09 (mac) to support the conclusion of this article should be sent to MF (fujikim@ms.naist.jp).

AUTHOR CONTRIBUTIONS

All the authors co-designed this work. MF, LW, and AJ co-wrote the paper. LW, NO, AJ, and MF co-measured and co-analyzed

the CPL, CPLE, CD, UV-visible, PL, and PLE spectra of Tb(fod)₃, Eu(fod)₃, Tb(dpm)₃, and Eu(dpm)₃ and other several lanthanide complexes in the presence of chiral additives and chiral solvents. LW and FA co-acquired and co-analyzed ss-¹³C{¹H}-FT-NMR and solution ¹H-NMR/¹⁹F-NMR spectra. FA conducted the elemental analysis of the products. MF performed MP2 and DFT calculations. LW, NO, AJ, AO, SO, HK, and MF contributed to a joint project of emerging CPL spectra from achiral organic, polymeric, and lanthanide luminophores endowed with chiral polymers and chiral solvents. All authors discussed the data and commented on the manuscript. All authors have given approval to the final version of the manuscript. These authors contributed equally. The manuscript was written through contributions of all authors.

FUNDING

MF thanks for the funding from Japan Society for the Promotion of Science (KAKENHI, 16H04155). AJ would like to acknowledge the support from the Fundamental Research Grant Scheme (FRGS) under a grant number of RACER/1/2019/TK05/UNIMAP//1 from the Ministry of Higher Education Malaysia.

ACKNOWLEDGMENTS

MF and AJ owe a debt of gratitude to Prof. Victor Borovcov (South-Central University for Nationalities, Wuhan, China) for giving us the opportunity to contribute to this special issue. LW and MF acknowledge Prof. Wei Zhang (Soochow University, China) for providing **D-Glu**. We thank Dr. Sibio Guo for assisting the chiroptical measurements. We thank Yoshiko Nishikawa for measuring and analyzing mass spectral data sets of **D-/L-Glu**, **D-/L-Ara**, Tb(fod)₃, Eu(fod)₃, Tb(dpm)₃, and Eu(dpm)₃, Yasuo Okajima for measuring photodynamics of Eu(fod)₃, Eu(dpm)₃, and Tb(dpm)₃ embedded to CTA and CABu specimens, and Prof. Tsuyoshi Ando for the permission to use Perkin Elmer FT-IR spectrometer.

SUPPLEMENTARY MATERIAL

The Supplementary Material for this article can be found online at: <https://www.frontiersin.org/articles/10.3389/fchem.2020.00685/full#supplementary-material> Characterization (¹H-/¹⁹F-NMR, CP-MAS-¹³C-FT-NMR, FT-IR, HR-ESI-MS spectra) of CTA, CABu, **D-/L-Glu**, **D-/L-Ara**, Eu(fod)₃, Tb(dpm)₃, and Eu(dpm)₃. Detailed measurement and analytical conditions of all instruments (solution ¹H-/¹⁹F-FT-NMR, solid-state CP-MAS-¹³C-FT-NMR). CPL/PL spectra of Eu(dpm)₃ in CABu and Eu(dpm)₃ in (S)-/(R)- α -pinene. Mulliken charges of **D-Glu dimer** obtained with MP2 (6-311 G basis set) calculation. Photodynamic decay curves of Eu(dpm)₃ in CTA, Eu(dpm)₃ in CABu, Eu(fod)₃ in CTA, Eu(fod)₃ in CABu, Tb(dpm)₃ in CTA, and Tb(dpm)₃ in CABu, raw CD and UV-visible spectra of Eu(fod)₃, Tb(fod)₃, and Tb(fod)₃ in CTA and CABu films and Eu(fod)₃ in **D-/L-Glu** and **D-/L-Glu** films.

REFERENCES

- Aida, T., Meijer, E. W., and Stupp, S. I. (2012). Functional supramolecular polymers. *Science* 335, 813–817. doi: 10.1126/science.1205962
- Akagi, K. (2019). Interdisciplinary chemistry based on integration of liquid crystals and conjugated polymers: development and progress. *Bull. Chem. Soc. Jpn.* 92, 1509–1655. doi: 10.1246/bcsj.20190092
- Bing, Y., Selassie, D., Paradise, R. H., Isborn, C., Kramer, N., Sadilek, M., et al. (2010). Circular dichroism tensor of a triarylmethyl propeller in sodium chlorate crystals. *J. Am. Chem. Soc.* 132, 7454–7465. doi: 10.1021/ja1018892
- Binnemans, K. (2015). Interpretation of europium(III) spectra. *Coord. Chem. Rev.* 295, 1–45. doi: 10.1016/j.ccr.2015.02.015
- Borovkov, V. (2014). Supramolecular chirality in porphyrin chemistry. *Symmetry* 6, 256–294. doi: 10.3390/sym6020256
- Borovkov, V. V., Hembury, G. A., and Inoue, Y. (2004). Origin, control, and application of supramolecular chirogenesis in bisporphyrin-based systems. *Acc. Chem. Res.* 37, 449–459. doi: 10.1021/ar0302437
- Bosnich, B. J. (1967). Asymmetric syntheses, asymmetric transformations, and asymmetric inductions in an optically active solvent. *J. Am. Chem. Soc.* 89, 6143–6148. doi: 10.1021/ja01000a025
- Brittain, H. G. (1980). Correlation of circularly polarized luminescence induced in Tb(dpm)₃ by chiral solvents with the absolute configuration of those solvents. *J. Am. Chem. Soc.* 102, 1207–1208. doi: 10.1021/ja00523a071
- Brittain, H. G. (1981). Optical activity induced in Terbium(III) Tris(Pyridine-2,6-Dicarboxylate) through association with certain chiral amino acids. *Inorg. Chem.* 20, 3007–3013. doi: 10.1021/ic50223a050
- Brittain, H. G. (1982). Studies of the pfeiffer effect developed in tris(pyridine-2,6-dicarboxylato)terbate(III) by phenylalkylamines, phenylalkylamino alcohols, and phenylalkylamino acids. *Inorg. Chem.* 21, 2955–2960. doi: 10.1021/ic00138a009
- Brittain, H. G. (1983). Chiral lanthanide complexes. *Coord. Chem. Rev.* 48, 243–276. doi: 10.1016/0010-8545(83)80004-6
- Brittain, H. G. (1984). Studies of the pfeiffer effect induced in tris(Pyridine-2,6-Dicarboxylato) terbate(III) by monosaccharide aldose sugars. *J. Chem. Soc. Dalton Trans.* 7, 1367–1370. doi: 10.1039/dt9840001367
- Brittain, H. G. (1989). Circularly polarized luminescence studies of chiral lanthanide complexes. *J. Coord. Chem.* 20, 331–347. doi: 10.1080/00958978909408175
- Brittain, H. G., and Richardson, F. S. (1977a). Circularly polarized emission studies on chiral and achiral europium(III) β -diketonate complexes in an optically active solvent. *J. Am. Chem. Soc.* 99, 65–70. doi: 10.1021/ja00443a014
- Brittain, H. G., and Richardson, F. S. (1977b). Circularly polarized emission studies on Tb³⁺ and Eu³⁺ complexes with potentially terdentate amino acids in aqueous solution. *Bioinorg. Chem.* 7, 233–243. doi: 10.1016/S0006-3061(00)80097-6
- Bünzli, J.-C. (2010). Lanthanide luminescence for biomedical analyses and imaging. *Chem. Rev.* 110, 2729–2755. doi: 10.1021/cr900362e
- Carr, R., Evans, N. H., and Parker, D. (2012). Lanthanide complexes as chiral probes exploiting circularly polarized luminescence. *Chem. Soc. Rev.* 41, 7673–7686. doi: 10.1039/c2cs35242g
- Colquhoun, H. M., Stoddart, J. F., and Williams, D. J. (1986). Second-sphere coordination: a novel role for molecular receptors. *Angew. Chem. Int. Ed. Engl.* 25, 487–507. doi: 10.1002/anie.198604873
- Coulate, T. (2016). *Food—The Chemistry of its Components*. 6th Edn. Cambridge: RSC.
- De La Cruz, J. A., Liu, Q., Senyuk, B., Frazier, A. W., Peddireddy, K., and Smalyukh, I. I. (2018). Cellulose-based reflective liquid crystal films as optical filters and solar gain regulators. *ACS Photon.* 5, 2468–2477. doi: 10.1021/acsp Photonics.8b00289
- de Queiroz, T. B., Botelho, M. B. S., Gonçalves, T. S., Dousti, M. R., and de Camargo, A. S. S. (2015). New fluorophosphate glasses co-doped with Eu³⁺ and Tb³⁺ as candidates for generating tunable visible light. *J. Alloys Compd.* 647, 315–321. doi: 10.1016/j.jallcom.2015.06.066
- Desiraju, G. R., and Steiner, T. (1999). *The Weak Hydrogen Bond: In Structural Chemistry and Biology*. Oxford: Oxford University Press.
- Di Bari, L., and Salvadori, P. (2005). Solution structure of chiral lanthanide complexes. *Coord. Chem. Rev.* 249, 2854–2879. doi: 10.1016/j.ccr.2005.03.006
- Di Pietro, S., and Di Bari, L. (2012). The structure of MLn(hfbc)₄ and a key to high circularly polarized luminescence. *Inorg. Chem.* 51, 12007–12014. doi: 10.1021/ic3018979
- Duan, P., Cao, H., Zhang, L., and Liu, M. (2014). Gelation induced supramolecular chirality: chirality transfer, amplification and application. *Soft Matter* 10, 5428–5448. doi: 10.1039/C4SM00507D
- Dubois, J. C., Barny, P. L., Mauzac, M., and Noel, C. (1998). *Handbook of Liquid Crystals, Fundamentals High Regular Weight Liquid Crystal*, Vol. 3. eds D. Demus, J. W. Goodby, G. W. Gray, H. S. Spiess, and V. Vill (New York, NY: Wiley-VCH), 207–269.
- Duong, S. T., and Fujiki, M. (2017). The origin of bisignate circularly polarized luminescence (CPL) spectra from chiral polymer aggregates and molecular camphor: anti-kasha's rule revealed by CPL excitation (CPLE) spectra. *Polym. Chem.* 8, 4673–4679. doi: 10.1039/C7PY00958E
- Eliel, E. L., and Wilen, S. H. (1994). “Chiroptical properties”, in *Stereochemistry of Organic Compounds*, eds E. L. Eliel, S. H. Wilen, and L. N. Mander (New York, NY: Wiley-Interscience), 991–1118.
- Frisch, M. J., Trucks, G. W., Schlegel, H. B., Scuseria, G. E., Robb, M. A., Cheeseman, J. R., et al. (2013). *Gaussian 09, Rev. D.,01*. Wallingford, CT: Gaussian, Inc.
- Fujiki, M. (2014). Supramolecular chirality: solvent chirality transfer in molecular chemistry and polymer chemistry. *Symmetry* 6, 677–703. doi: 10.3390/sym6030677
- Fujiki, M., and Yoshimoto, S. (2017). Time-evolved, far-red, circularly polarised luminescent polymer aggregates endowed with sacrificial helical Si–Si bond polymers. *Mater. Chem. Front.* 1, 1773–1785. doi: 10.1039/C7QM00096K
- Fulgêncio, F., de Oliveira, F. C., Windmüller, D., Brito, H. F., Malta, O. L., de Sá, G. F., et al. (2012). Evidence of the participation of electronic excited states in the mechanism of positronium formation in substitutional Tb_{1-x}Eu_x(dpm)₃ solid solutions studied by optical and positron annihilation spectroscopies. *Phys. Chem. Chem. Phys.* 14, 9996–10007. doi: 10.1039/c2cp40664k
- George, S. J., Tomovic, Z., Schenning, A. P. H. J., and Meijer, E. W. (2011). Insight into the chiral induction in supramolecular stacks through preferential chiral solvation. *Chem. Commun.* 47, 3451–3453. doi: 10.1039/c0cc04617e
- Glover-Fischer, D. P., Metcalf, D. H., Hopkins, T. A., Pugh, V. J., Chisdes, S. J., Kankare, J., et al. (1998). Excited-state enantiomer interconversion kinetics probed by time-resolved chiroptical luminescence spectroscopy. the solvent and temperature dependence of Δ -Eu(dpa)₃³⁻ \rightleftharpoons Λ -Eu(dpa)₃³⁻ enantiomer interconversion rates in solution. *Inorg. Chem.* 37, 3026–3033. doi: 10.1021/ic9713700
- Goto, T., Okazaki, Y., Ueki, M., Kuwahara, Y., Takafuji, M., Oda, R., et al. (2017). Induction of strong and tunable circularly polarized luminescence of nonchiral, nonmetal, low-molecular-weight fluorophores using chiral nanotemplates. *Angew. Chem. Int. Ed.* 56, 2989–2993. doi: 10.1002/anie.201612331
- Green, M. M., Khatri, C., and Peterson, N. C. (1993). A macromolecular conformational change driven by a minute chiral solvation energy. *J. Am. Chem. Soc.* 115, 4941–4942. doi: 10.1021/ja00064a086
- Guo, G., Suzuki, N., and Fujiki, M. (2017). Oligo- and polyfluorenes meet cellulose alkyl esters: retention, inversion, and racemization of circularly polarized luminescence (CPL) and circular dichroism (CD) via intermolecular C–H/O=C interactions. *Macromolecules* 50, 1778–1789. doi: 10.1021/acs.macromol.6b02762
- Guo, S., Kamite, H., Suzuki, N., Wang, L., Ohkubo, A., and Fujiki, M. (2018). Ambidextrous chirality transfer capability from cellulose tris(phenylcarbamate) to nonhelical chainlike luminophores: achiral solvent-driven helix-helix transition of oligo- and polyfluorenes revealed by sign inversion of circularly polarized luminescence and circular dichroism spectra. *Biomacromolecules* 19, 449–459. doi: 10.1021/acs.biomac.7b01554
- Hayward, L. D., and Totty, R. N. (1969). Induced optical rotation and circular dichroism of symmetric and racemic aliphatic carbonyl compounds. *J. Chem. Soc. D. Chem. Commun.* 676–677. doi: 10.1039/c29690000676
- Head-Gordon, M., Pople, J. A., and Frisch, M. J. (1988). MP2 energy evaluation by direct methods. *Chem. Phys. Lett.* 153, 503–506. doi: 10.1016/0009-2614(88)85250-3

- Hembury, G. A., Borovkov, V. V., and Inoue, Y. (2008). Chirality-sensing supramolecular systems. *Chem. Rev.* 108, 1–73. doi: 10.1021/cr050005k
- Henriksson, M., Henriksson, G., Berglund, L. A., and Lindström, T. (2007). An environmentally friendly method for enzyme-assisted preparation of microfibrillated cellulose (MFC) nanofibers. *Eur. Polym. J.* 43, 3434–3441. doi: 10.1016/j.eurpolymj.2007.05.038
- Huang, X., Rickman, B. H., Borhan, B., Berova, N., and Nakanishi, K. (1998). Zinc porphyrin tweezer in host–guest complexation: determination of absolute configurations of diamines, amino acids, and amino alcohols by circular dichroism. *J. Am. Chem. Soc.* 120, 6185–6186. doi: 10.1021/ja973539e
- Huskowska, E., and Riehl, J. P. (1995). Perturbation of the racemic equilibrium between d_3 lanthanide complexes through the addition of sugars. *Inorg. Chem.* 34, 5615–5621. doi: 10.1021/ic00126a035
- Ikai, T., and Okamoto, Y. (2009). Structure control of polysaccharide derivatives for efficient separation of enantiomers by chromatography. *Chem. Rev.* 109, 6077–6101. doi: 10.1021/cr8005558
- Isare, B., Linares, M., Zargarian, L., Fermandjian, S., Miura, M., Motohashi, S., et al. (2010). Chirality in dynamic supramolecular nanotubes induced by a chiral solvent. *Chem. Eur. J.* 16, 173–177. doi: 10.1002/chem.200902399
- Iwamura, M., Kimura, Y., Miyamoto, R., and Nozaki, K. (2012). Chiral sensing using an achiral europium(III) complex by induced circularly polarized luminescence. *Inorg. Chem.* 51, 4094–4098. doi: 10.1021/ic202355s
- Iwamura, M., Uchida, T.-A., and Nozaki, K. (2016). Chiral sensing of various amino acids using induced circularly polarized luminescence from europium(III) complexes of phenanthroline dicarboxylic acid derivatives. *Chem. Asian J.* 11, 2415–2422. doi: 10.1002/asia.201600798
- Iwatake, A., Nogi, M., and Yano, H. (2008). Cellulose nanofiber-reinforced polylactic acid. *Compos. Sci. Technol.* 68, 2103–2106. doi: 10.1016/j.compscitech.2008.03.006
- Jacoby, M. (2008). Recognizing a pioneer. *Chem. Eng. News* 86, 38–41. doi: 10.1021/cen-v086n033.p038
- Jalilah, A. J., Asanoma, F., and Fujiki, M. (2018). Unveiling controlled breaking of the mirror symmetry of $\text{Eu}(\text{Fod})_3$ with α - β -pinene and BINAP by circularly polarized luminescence (CPL), CPL excitation, and ^{19}F - $^{31}\text{P}\{^1\text{H}\}$ -NMR spectra and Mulliken charges. *Inorg. Chem. Front.* 5, 2718–2733. doi: 10.1039/C8QJ00509E
- Jiang, S., Zhao, Y., Wang, L., Yin, L., Zhang, Z., Zhu, J., et al. (2015). Photocontrollable induction of supramolecular chirality in achiral side chain azo-containing polymers through preferential chiral solvation. *Polym. Chem.* 6, 4230–4239. doi: 10.1039/C5PY00496A
- Kahr, B., and Gurney, R. W. (2001). Dyeing crystals. *Chem. Rev.* 101, 893–951. doi: 10.1021/cr980088n
- Kawagoe, Y., Fujiki, M., and Nakano, Y. (2010). Limonene magic: noncovalent molecular chirality transfer leading to ambidextrous circularly polarized luminescent π -conjugated polymers. *New J. Chem.* 34, 637–647. doi: 10.1039/b9nj00733d
- Khorasaninejad, M., Chen, W. T., Zhu, A. Y., Oh, J., Devlin, R. C., Rousso, D., et al. (2016). Multispectral chiral imaging with a metalens. *Nano Lett.* 16, 4595–4600. doi: 10.1021/acs.nanolett.6b01897
- Kim, S. Y., Saxena, A., Kwak, G., Fujiki, M., and Kawakami, Y. (2004). Cooperative C–F...Si interaction in optically active helical polysilanes. *Chem. Commun.* 2004, 538–539. doi: 10.1039/b314723a
- Kipping, F. S., and Pope, W. J. (1898). LXIII.—enantiomorphism. *J. Chem. Soc., Trans.* 73, 606–617. doi: 10.1039/CT8987300606
- Kirschner, S., and Ahmad, M. (1968). The Application of the Pfeiffer effect to the resolution of dissymmetric coordination compounds. *J. Am. Chem. Soc.* 90, 1910–1911. doi: 10.1021/ja01009a047
- Kirschner, S., and Bakkar, I. (1982). Utilization of the Pfeiffer effect and outer-sphere complexation for the prediction of absolute configurations of optically active metal complexes. *Coord. Chem. Rev.* 43, 325–335. doi: 10.1016/S0010-8545(00)82103-7
- Klemm, D., Heublein, B., Fink, H.-P., and Bohn, A. (2005). Cellulose: fascinating biopolymer and sustainable raw material. *Angew. Chem. Int. Ed.* 44, 3358–3393. doi: 10.1002/anie.200460587
- Kobayashi, K., Asakawa, Y., Kikuchi, Y., Toi, H., and Aoyama, Y. (1993). CH- π interaction as an important driving force of host-guest complexation in apolar organic media. binding of monools and acetylated compounds to resorcinol cyclic tetramer as studied by ^1H NMR and circular dichroism spectroscopy. *J. Am. Chem. Soc.* 115, 2648–2654. doi: 10.1021/ja00060a013
- Koiso, N., Kitagawa, Y., Nakanishi, T., Fushimi, K., and Hasegawa, Y. (2017). Eu(III) Chiral coordination polymer with a structural transformation system. *Inorg. Chem.* 56, 5741–5747. doi: 10.1021/acs.inorgchem.7b00337
- Kono, Y., Nakabayashi, K., Kitamura, S., Shizuma, M., Fujiki, M., and Imai, Y. (2016). Can chiral P(III) coordinate Eu(III)? unexpected solvent dependent circularly polarized luminescence of BINAP and Eu(III)(hfa) $_3$ in chloroform and acetone. *RSC Adv.* 6, 40219–40224. doi: 10.1039/C6RA05856F
- Kruk, S. S., Decker, M., Staude, I., Schlecht, S., Greppmair, M., Neshev, D. N., et al. (2014). Spin-polarized photon emission by resonant multipolar nanoantennas. *ACS Photonics* 1, 1218–1223. doi: 10.1021/ph500288u
- Kumar, J., Nakashima, T., and Kawai, T. (2015). Circularly polarized luminescence in chiral molecules and supramolecular assemblies. *J. Phys. Chem. Lett.* 6, 3445–3452. doi: 10.1021/acs.jpcllett.5b01452
- Lee, D., Jin, Y.-J., Suzuki, N., Fujiki, M., Sakaguchi, T., Kim, S., et al. (2012). Solvent-to-polymer chirality transfer in intramolecular stack structure. *Macromolecules* 45, 5379–5386. doi: 10.1021/ma300976r
- Leonzio, M., Melchior, A., Faura, G., Tolazzi, M., Zinna, F., Di Bari, L., et al. (2017). Strongly circularly polarized emission from water-soluble Eu(III)- and Tb(III)-based complexes: a structural and spectroscopic study. *J. Am. Chem. Soc.* 139, 4413–4421. doi: 10.1021/acs.inorgchem.7b00430
- Liu, M., Zhang, L., and Wang, T. (2015). Supramolecular chirality in self-assembled systems. *Chem. Rev.* 115, 7304–7397. doi: 10.1021/cr500671p
- Longhi, G., Castiglioni, E., Koshoubu, J., Mazzeo, G., and Abbate, S. (2016). Circularly polarized luminescence: a review of experimental and theoretical aspects. *Chirality* 28, 696–707. doi: 10.1002/chir.22647
- Luk, C. K., and Richardson, F. S. (1974). Circularly polarized luminescence of terbium (III) complexes in solution. *Chem. Phys. Lett.* 25, 215–220. doi: 10.1016/0009-2614(74)89121-9
- Lunkley, J. L., Nguyen, N. M., Tuminaro, K. M., Margittai, D., and Muller, G. (2018). The importance of solvent effects on the mechanism of the Pfeiffer effect. *Inorganics* 6, 87. doi: 10.3390/inorganics6030087
- Lunkley, J. L., Shirotani, D., Yamanari, K., Kaizaki, S., and Muller, G. (2008). Extraordinary circularly polarized luminescence activity exhibited by cesium Tetrakis(3-heptafluorobutylryl-(-)-camphorato) Eu(III) complexes in EtOH and CHCl_3 solutions. *J. Am. Chem. Soc.* 130, 13814–13815. doi: 10.1021/ja805681w
- Madaras, J. S., and Brittain, H. G. (1980). Induced optical activity in the Tb(III) complex of Pyridine-2,6-Dicarboxylic acid through outer-sphere coordination with L-Ascorbic acid. *Inorg. Chim. Acta* 42, 109–113. doi: 10.1016/S0020-1693(00)88894-5
- Mahadevi, A. S., and Sastry, G. N. (2016). Cooperativity in noncovalent interactions. *Chem. Rev.* 116, 2775–2825. doi: 10.1021/cr500344e
- Mason, S. F. (1982). *Molecular Optical Activity and the Chiral Discrimination*, 353–367, Cambridge: Cambridge University Press, 208–210.
- Mason, S. F., and Norman, B. J. (1965). Outer-sphere co-ordination and optical activity in transition-metal complexes. *Chem. Commun.* 335–336. doi: 10.1039/c19650000335
- Matsuura, H., Yoshida, H., Hieda, M., Yamanaka, S.-Y., Harada, T., Shin-ya, K., et al. (2003). Experimental evidence for intramolecular blue-shifting C–H...O hydrogen bonding by matrix-isolation infrared spectroscopy. *J. Am. Chem. Soc.* 125, 13910–13911. doi: 10.1021/ja030538f
- Mayer, L. A., and Brasted, R. C. (1973). Further evidence on the origins of the Pfeiffer effect using circular dichroism. *J. Coord. Chem.* 3, 85–89. doi: 10.1080/00958977308073791
- Mei, J., Leung, N. L. C., Kwok, R. T. K., Lam, J. W. Y., and Tang, B. Z. (2015). Aggregation-induced emission: together we shine, united we soar! *Chem. Rev.* 115, 11718–11940. doi: 10.1021/acs.chemrev.5b00263
- Mele, A., Tran, C. D., and De Pauli Lacerda, S. H. (2003). The structure of a room-temperature ionic liquid with and without trace amounts of water: the role of C–H...O and C–H...F interactions in 1-n-Butyl-3-methylimidazolium tetrafluoroborate. *Angew. Chem. Int. Ed.* 42, 4364–4366. doi: 10.1002/anie.200351783
- Miyake, H. (2014). Supramolecular chirality in dynamic coordination chemistry. *Symmetry* 6, 880–895. doi: 10.3390/sym6040880

- Miyake, H., Terada, K., and Tsukube, H. (2014). Lanthanide Tris(β -diketonates) as useful probes for chirality determination of biological amino alcohols in vibrational circular dichroism: ligand to ligand chirality transfer in lanthanide coordination sphere. *Chirality* 26, 293–299. doi: 10.1002/chir.22319
- Møller, C., and Plesset, M. S. (1934). Note on an approximation treatment for many-electron systems. *Phys. Rev.* 46, 618–622. doi: 10.1103/PhysRev.46.618
- Muller, G. (2009). Luminescent chiral lanthanide (III) complexes as potential molecular probes. *Dalton Trans.* 9692–9707. doi: 10.1039/b909430j
- Muller, G. (2014). “Circularly polarised luminescence,” in *Luminescence of Lanthanide Ions in Coordination Compounds and Nanomaterials*, ed A. de Bettencourt-Dias (Chichester: Wiley), 77–123. doi: 10.1002/9781118682760.ch03
- Muller, G., and Riehl, J. P. (2005). Use of induced circularly polarized luminescence (CPL) from racemic D_3 lanthanide complexes to determine the absolute configuration of amino acids. *J. Fluor.* 15, 553–558. doi: 10.1007/s10895-005-2828-4
- Mulliken, R. S. (1955). Electronic population analysis on LCAO–MO molecular wave functions. *I. J. Chem. Phys.* 23, 1833–1840. doi: 10.1063/1.1740588
- Murray-Rust, P., Stallings, W. C., Monti, C. T., Preston, R. K., and Glusker, J. P. (1983). Intermolecular interactions of the C–F bond: The crystallographic environment of fluorinated carboxylic acids and related structures. *J. Am. Chem. Soc.* 105, 3206–3214. doi: 10.1021/ja00348a041
- Nakano, Y., and Fujiki, M. (2011). Circularly polarized light enhancement by helical polysilane aggregates suspension in organic optofluid. *Macromolecules* 44, 7511–7519. doi: 10.1021/ma201665n
- Nakano, Y., Ichiyanagi, F., Naito, M., Yang, Y., and Fujiki, M. (2012). Chiroptical generation and inversion during the mirror-symmetry-breaking aggregation of dialkylpolysilanes due to limonene chirality. *Chem. Commun.* 48, 6636–6638. doi: 10.1039/c2cc17845a
- Nakano, Y., Liu, Y., and Fujiki, M. (2010). Ambidextrous circular dichroism and circularly polarised luminescence from Poly(9,9-di-*n*-decylfluorene) by terpene chirality transfer. *Polym. Chem.* 1, 460–469. doi: 10.1039/B9PY00288J
- Nakashima, H., Koe, J. R., Torimitsu, K., and Fujiki, M. (2001). Transfer and amplification of chiral molecular information to polysilylene aggregates. *J. Am. Chem. Soc.* 123, 4847–4848. doi: 10.1021/ja010119n
- Nishio, M., Hirota, M., and Umezawa, Y. (1998). *The CH/ π Interaction. Evidence, Nature, and Consequences*. New York, NY: Wiley-VCH.
- Noack, K. (1969). Induktion von circulardichroismus in einer optisch inaktiven Verbindung durch zwischenmolekulare Wechselwirkung mit einem optisch aktiven Lösungsmittel. *Helv. Chim. Acta* 52, 2501–2507. doi: 10.1002/hlca.19690520833
- Numata, N., and Shinkai, S. (2011). ‘Supramolecular wrapping chemistry’ by helix-forming polysaccharides: a powerful strategy for generating diverse polymeric nano-architectures. *Chem. Commun.* 47, 1961–1975. doi: 10.1039/c0cc03133j
- Onofrei, M. D., Dobos, A. M., and Ioan, S. (2015). In *Polymer Nanocomposites: Fundamentals and Applications* ed V. K. Thakur (Weinheim: Wiley), 355–391.
- Palmans, A. R. A., and Meijer, E. W. (2007). Amplification of chirality in dynamic supramolecular aggregates. *Angew. Chem. Int. Ed.* 46, 8948–8968. doi: 10.1002/anie.200701285
- Pearson, R. G. (1963). Hard and soft acids and bases. *J. Am. Chem. Soc.* 85, 3533–3539. doi: 10.1021/ja00905a001
- Perucca, E. (1919). Nuove osservazioni e misure su cristalli otticamente attivi (NaClO_3). *II Nuovo Cimento*, 18, 112–154. doi: 10.1007/BF02959865
- Petoud, S., Muller, G., Moore, E. G., Xu, J., Sokolnicki, J., Riehl, J. P., et al. (2007). Brilliant Sm, Eu, Tb, and Dy chiral lanthanide complexes with strong circularly polarized luminescence. *J. Am. Chem. Soc.* 129, 77–83. doi: 10.1021/ja064902x
- Pfeiffer, P., and Quehl, K. (1931). Über einen neuen effekt in lösungen optischaktiver substanzen (I. Mitteil). *Chem. Ber.* 64, 2667–2671. doi: 10.1002/cber.19310641015
- Pfeiffer, P., and Quehl, K. (1932). Aktivierung von Komplexsalzen in wässriger Lösung (II. Mitteil). *Chem. Ber.* 65, 560–565. doi: 10.1002/cber.19320650410
- Pitts, C. R., Siegler, M. A., and Lectka, T. (2017). Intermolecular aliphatic C–F...H–C interaction in the presence of “stronger” hydrogen bond acceptors: crystallographic, computational, and IR studies. *J. Org. Chem.* 82, 3996–4000. doi: 10.1021/acs.joc.7b00268
- Prince, R. B., Barnes, S. A., and Moore, J. S. (2000). Foldamer-based molecular recognition. *J. Am. Chem. Soc.* 122, 2758–2762. doi: 10.1021/ja993830p
- Richardson, F. S. (1982). Terbium(III) and europium(III) Ions as luminescent probes and stains for biomolecular systems. *Chem. Rev.* 82, 541–552. doi: 10.1021/cr00051a004
- Riehl, J. P., and Richardson, F. S. (1986). Circularly polarized luminescence spectroscopy. *Chem. Rev.* 86, 1–16. doi: 10.1021/cr00071a001
- Roose, J., Tang, B. Z., and Wong, K. S. (2016). Circularly-polarized luminescence (CPL) from chiral AIE molecules and macrostructures. *Small* 12, 6495–6512. doi: 10.1002/smll.201601455
- Sang, Y., Han, Y. J., Zhao, T., Duan, P. and Liu, M. (2019). Circularly polarized luminescence in nanoassemblies: generation, amplification, and application. *Adv. Mater.* doi: 10.1002/adma.201900110. [Epub ahead of print].
- Schipper, P. E. (1975). On the chemical consequences of long-range interactions in chiral systems. *Aust. J. Chem.* 28, 1161–1168. doi: 10.1071/CH9751161
- Schipper, P. E. (1978). Induced equilibrium shifts in labile racemates. The nature of the discriminatory interactions in the Pfeiffer effect. *J. Am. Chem. Soc.* 100, 1079–1084. doi: 10.1021/ja00472a010
- Soai, K., Kawasaki, T., and Matsumoto, A. (2019). Role of asymmetric autocatalysis in the elucidation of origins of homochirality of organic compounds. *Symmetry* 11:694. doi: 10.3390/sym11050694
- Tanaka, H., Ikenosako, M., Kato, Y., Fujiki, M., Inoue, Y., and Mori, T. (2018). Symmetry-based rational design for boosting chiroptical responses. *Comm. Chem.* 1:38. doi: 10.1038/s42004-018-0035-x
- Taniguchi, A., Hara, N., Shizuma, M., Tajima, N., Fujiki, M., and Imai, Y. (2019). Circularly polarised luminescence from planar-chiral phanephos/Tb(III)(hfa)₃ hybrid luminophores. *Photochem. Photobiol. Sci.* 18, 2859–2864. doi: 10.1039/C9PP00296K
- Tanner, P. A. (2013). Some misconceptions concerning the electronic spectra of tri-positive europium and cerium. *Chem. Soc. Rev.* 42, 5090–5101. doi: 10.1039/c3cs60033e
- Tsukube, H., and Shinoda, S. (2002). Lanthanide complexes in molecular recognition and chirality sensing of biological substrates. *Chem. Rev.* 102, 2389–2403. doi: 10.1021/cr010450p
- Tsuzuki, S., Uchamaru, T., Mikami, M., and Urata, S. (2003). Ab Initio calculations of intermolecular interaction of CHF_3 dimer: origin of attraction and magnitude of CH/F interaction. *J. Phys. Chem. A* 107, 7962–7968. doi: 10.1021/jp035531z
- Wang, L., Suzuki, N., Liu, J., Matsuda, T., Abdul Rahim, N. A., Zhang, W., et al. (2014). Limonene induced chiroptical generation and inversion during aggregation of achiral polyfluorene analogs: structure-dependence and mechanism. *Polym. Chem.* 5, 5920–5920. doi: 10.1039/C4PY00865K
- Wang, L., Yin, L., Zhang, W., Zhu, X., and Fujiki, M. (2017). Circularly polarized light with sense and wavelengths to regulate azobenzene supramolecular chirality in optofluidic medium. *J. Am. Chem. Soc.* 139, 13218–13226. doi: 10.1021/jacs.7b07626
- Wang, Z., Teh, B. H., Wang, Y., Adamo, G., Teng, J., and Sun, H. (2007). Enhancing circular dichroism by super chiral hot spots from a chiral metasurface with apices. *Appl. Phys. Lett.* 110, 221108. doi: 10.1063/1.4984920
- Wilts, B. D., Dumanli, A. G., Middleton, R., Vukusic, P., and Vignolini, S. (2017). Chiral optics of helicoidal cellulose nanocrystal films. *APL Photonics* 2:040801. doi: 10.1063/1.4978387
- Wong, H.-Y., Lo, W.-S., Yim, K.-H., and Law, G.-L. (2019). Chirality and chiroptics of lanthanide molecular and supramolecular assemblies. *Chem* 5, 3058–3095. doi: 10.1016/j.chempr.2019.08.006
- Wormald, M. R., Petrescu, A. J., Pao, J.-L., Glithero, A., Elliott, T., and Dwek, R. (2002). A conformational studies of oligosaccharides and glycopeptides: complementarity of NMR, X-ray crystallography, and molecular modelling. *Chem. Rev.* 102, 371–386. doi: 10.1021/cr990368i
- Wu, S., Hilmes, G. L., and Riehl, J. P. (1989). Nature of chiral-induced equilibrium shifts in racemic labile lanthanide complexes. *J. Phys. Chem.* 93, 2307–2310. doi: 10.1021/j100343a022
- Wu, T., and Bouř, P. (2018). Specific circularly polarized luminescence of Eu(III), Sm(III), and Er(III) induced by *N*-acetylneuraminic acid. *Chem. Commun.* 54, 1790–1792. doi: 10.1039/C7CC09463A
- Wu, T., Bouř, P., and Andrushchenko, V. (2019). Europium (III) as a circularly polarized luminescence probe of DNA structure. *Sci. Rep.* 9:1068. doi: 10.1038/s41598-018-37680-7
- Wu, T., Průša, J., Kessler, J., Dračinský, M., Valenta, J., and Bour, P. (2016). Detection of sugars via chirality induced in europium(III)

- compounds. *Anal. Chem.* 88, 8878–8885. doi: 10.1021/acs.analchem.6b02505
- Xue, X., Cheng, T., Suzuki, T., and Ohishi, Y. (2015). Upconversion emissions from high energy levels of Tb³⁺ under near-infrared laser excitation at 976 nm. *Opt. Mater. Exp.* 5, 2768–2776. doi: 10.1364/OME.5.002768
- Yamada, T., Nomura, K., and Fujiki, M. (2018). Noticeable chiral center dependence of signs and magnitudes in circular dichroism (CD) and circularly polarized luminescence (CPL) spectra of all-trans poly(9,9-dialkylfluorene-2,7-vinylene)s bearing chiral alkyl side chains in solution, aggregates, and in thin films. *Macromolecules* 51, 2377–2387. doi: 10.1021/acs.macromol.8b00241
- Yan, F., Copeland, R. A., and Brittain, H. G. (1982). Optical activity induced in the terbium(III) and europium(III) tris complexes of pyridine-2,6-dicarboxylate through association with monoamino- and diamino-carboxylic acids. *Inorg. Chem.* 21, 1180–1185. doi: 10.1021/ic00133a059
- Yang, X., Lin, X., Zhao, Y., Zhao, Y. S., and Yan, D. (2017). Lanthanide metal-organic framework microrods: colored optical waveguides and chiral polarized emission. *Angew. Chem. Int. Ed.* 56, 7853–7857. doi: 10.1002/anie.201703917
- Yashima, E., Matsushima, T., and Okamoto, Y. (1995). Poly((4-carboxyphenyl)acetylene) as a probe for chirality assignment of amines by circular dichroism. *J. Am. Chem. Soc.* 117, 11596–11597. doi: 10.1021/ja00151a032
- Yeung, C.-T., Yim, K.-H., Wong, H.-Y., Pal, R., Lo, W.-S., Yan, S.-C., et al. (2017). Chiral transcription in self-assembled tetrahedral Eu₄L₆ chiral cages displaying sizable circularly polarized luminescence. *Nat. Commun.* 8:1128. doi: 10.1038/s41467-017-01025-1
- Yu, H., Pan, K., and Deng, J. (2018). Cellulose concurrently induces predominantly one-handed helicity in helical polymers and controls the shape of optically active particles thereof. *Macromolecules* 51, 5656–5664. doi: 10.1021/acs.macromol.8b01282
- Yu, Y., Gim, S., Kim, D., Arnon, Z. A., Gazit, E., Seeberger, P. H., et al. (2019). Oligosaccharides self-assemble and show intrinsic optical properties. *J. Am. Chem. Soc.* 2019, 141, 4833–4838. doi: 10.1021/jacs.8b11882
- Yuasa, J., Ohno, T., Miyata, K., Tsumatori, H., Hasegawa, Y., and Kawai, T. (2011). Noncovalent ligand-to-ligand interactions alter sense of optical chirality in luminescent Tris(β -diketonate) Lanthanide(III) complexes containing a chiral bis(oxazolonyl) pyridine ligand. *J. Am. Chem. Soc.* 133, 9892–9902. doi: 10.1021/ja201984u
- Zheng, H., Li, W., Li, W., Wang, X., Tang, Z., Zhang, S. X.-A., et al. (2018). Uncovering the circular polarization potential of chiral photonic cellulose films for photonic applications. *Adv. Mater.* 30:1705948. doi: 10.1002/adma.201705948
- Zhou, Y., Li, H., Zhu, T., Gao, T., and Yan, P. A. (2019). Highly luminescent chiral tetrahedral Eu₄L₄(L)₄ cage: chirality induction, chirality memory, and circularly polarized luminescence. *J. Am. Chem. Soc.* 141, 19634–19643. doi: 10.1021/jacs.9b07178
- Zinna, F., and Di Bari, L. (2015). Lanthanide circularly polarized luminescence: bases and applications. *Chirality* 27, 1–13. doi: 10.1002/chir.22382
- Zou, C., Qu, D., Jiang, H., Lu, D., Ma, X., Zhao, Z., et al. (2019). Bacterial cellulose: a versatile chiral host for circularly polarized luminescence. *Molecules* 24:1008. doi: 10.3390/molecules24061008

Conflict of Interest: The authors declare that the research was conducted in the absence of any commercial or financial relationships that could be construed as a potential conflict of interest.

Copyright © 2020 Fujiki, Wang, Ogata, Asanoma, Okubo, Okazaki, Kamite and Jalilah. This is an open-access article distributed under the terms of the Creative Commons Attribution License (CC BY). The use, distribution or reproduction in other forums is permitted, provided the original author(s) and the copyright owner(s) are credited and that the original publication in this journal is cited, in accordance with accepted academic practice. No use, distribution or reproduction is permitted which does not comply with these terms.